第4回
火星の水と気候変動

過去の火星の気候

表面地形から、過去のある時期に液体の水が地表に存在していたことが示唆される。この頃の火星は液体の水が地表に存在できる程度に温暖で湿潤であった可能性がある。

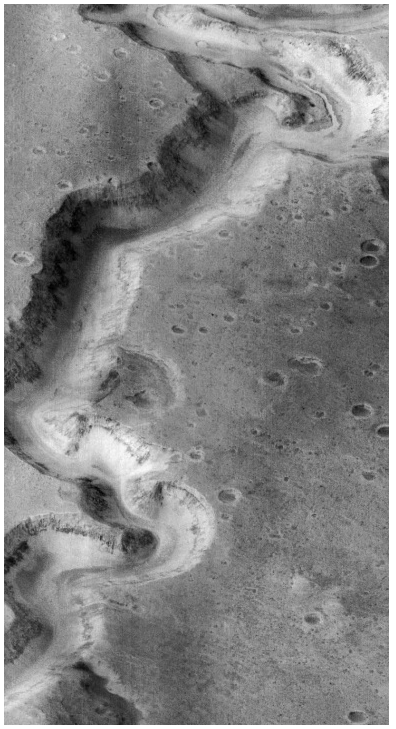

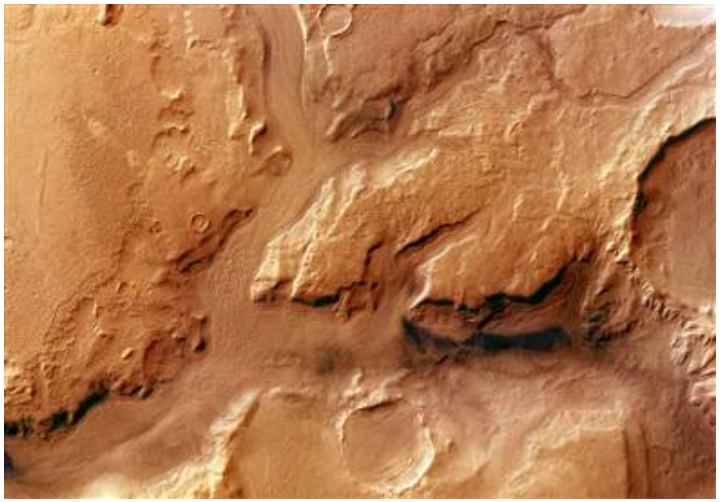

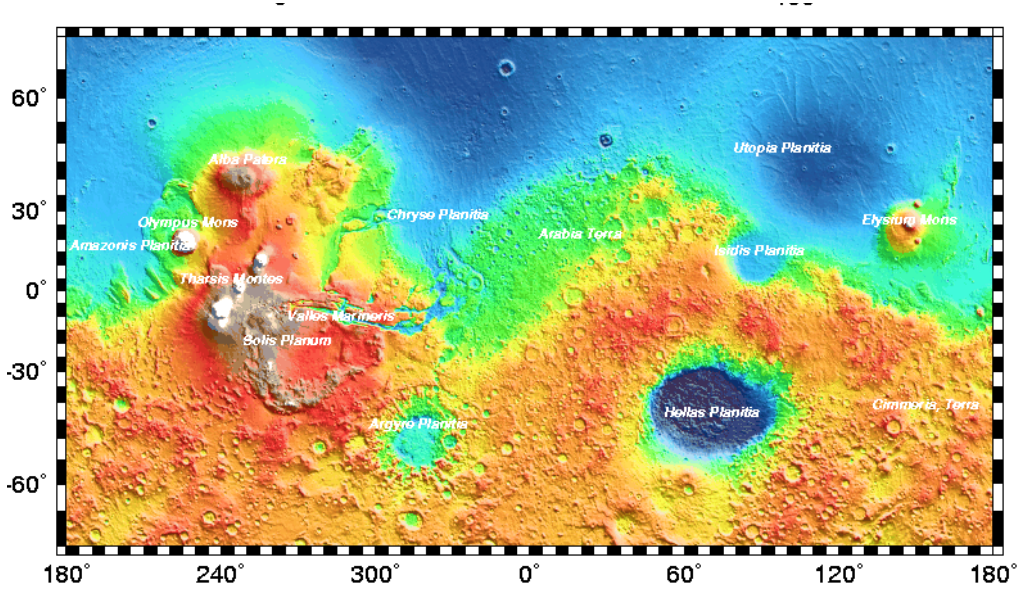

火星の歴史

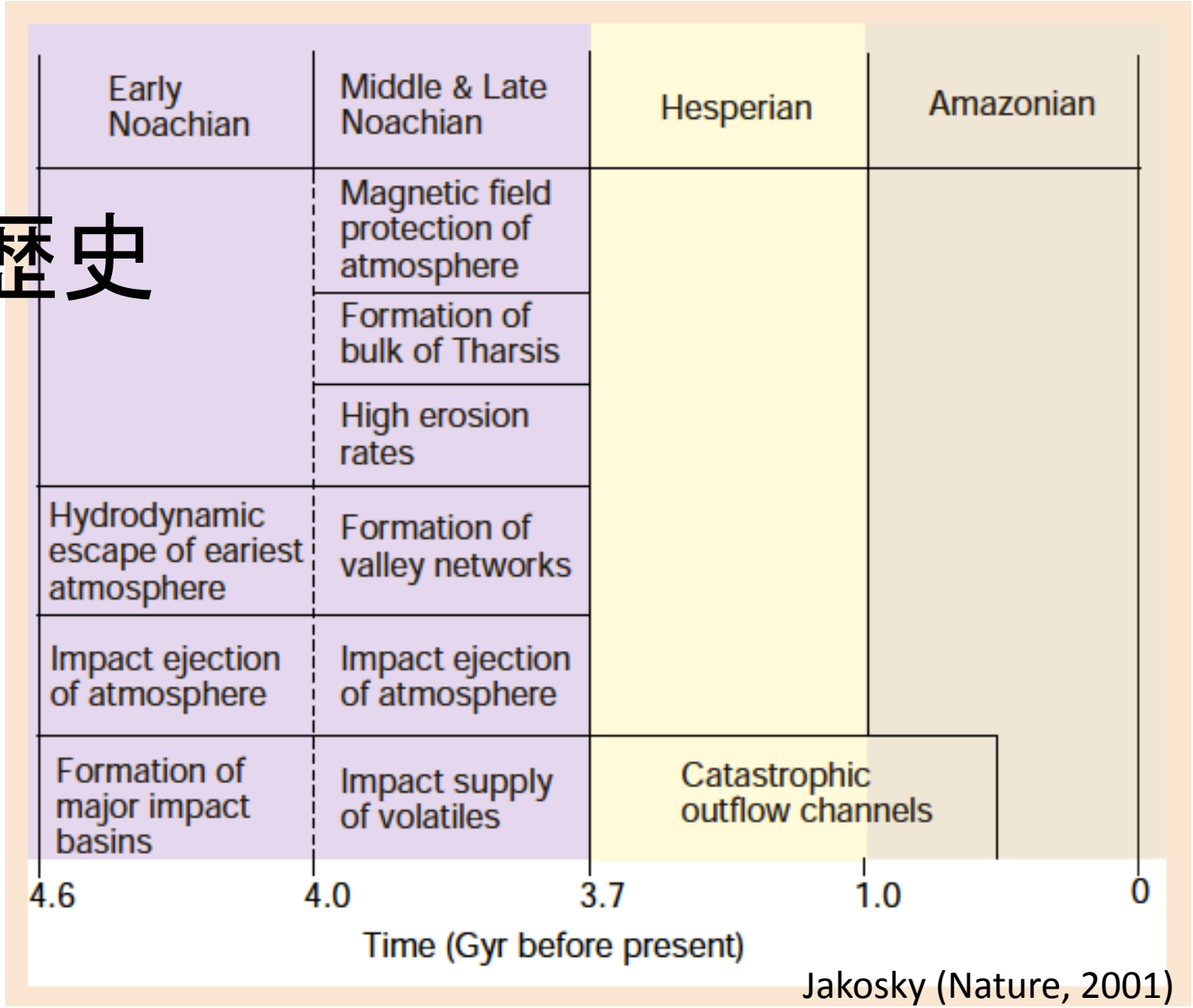

Jakosky (Nature, 2001)

- Noachian期には地表に液体の水が存在したと思われる
- 数気圧のCO_2があればそのような温暖な気候になりうる

同位体比と大気散逸

Table 1 Martian isotope ratios and atmospheric loss*

Isotope ratio	Measured value†	Amount lost to space (%)‡
D/H	5	~60–74
$^{38}Ar/^{36}Ar$	1.3	~50–90
$^{13}C/^{12}C$	1.05–1.07	~50–90
$^{15}N/^{14}N$	1.7	~90
$^{18}O/^{16}O$	1.025	~25–50

*Values taken from refs 57–59, 62, 77 and 78, and references therein.
†Value estimated, observed or derived for martian atmosphere relative to terrestrial.
‡Calculated assuming Rayleigh fractionation. D/H range includes uncertainty in escape processes. Other ranges are based on uncertain timing of outgassing relative to escape.

Jakosky (Nature, 2001)

- かなりの大気成分が宇宙に逃げた可能性がある
- CO2、SO2（これも温室効果気体）はそれぞれ炭酸塩・硫酸塩となって地下に残されている可能性がある

Mars Odyssey

Neutron Spectrometer (NS) and High-Energy Neutron Detector (HEND)

地下氷

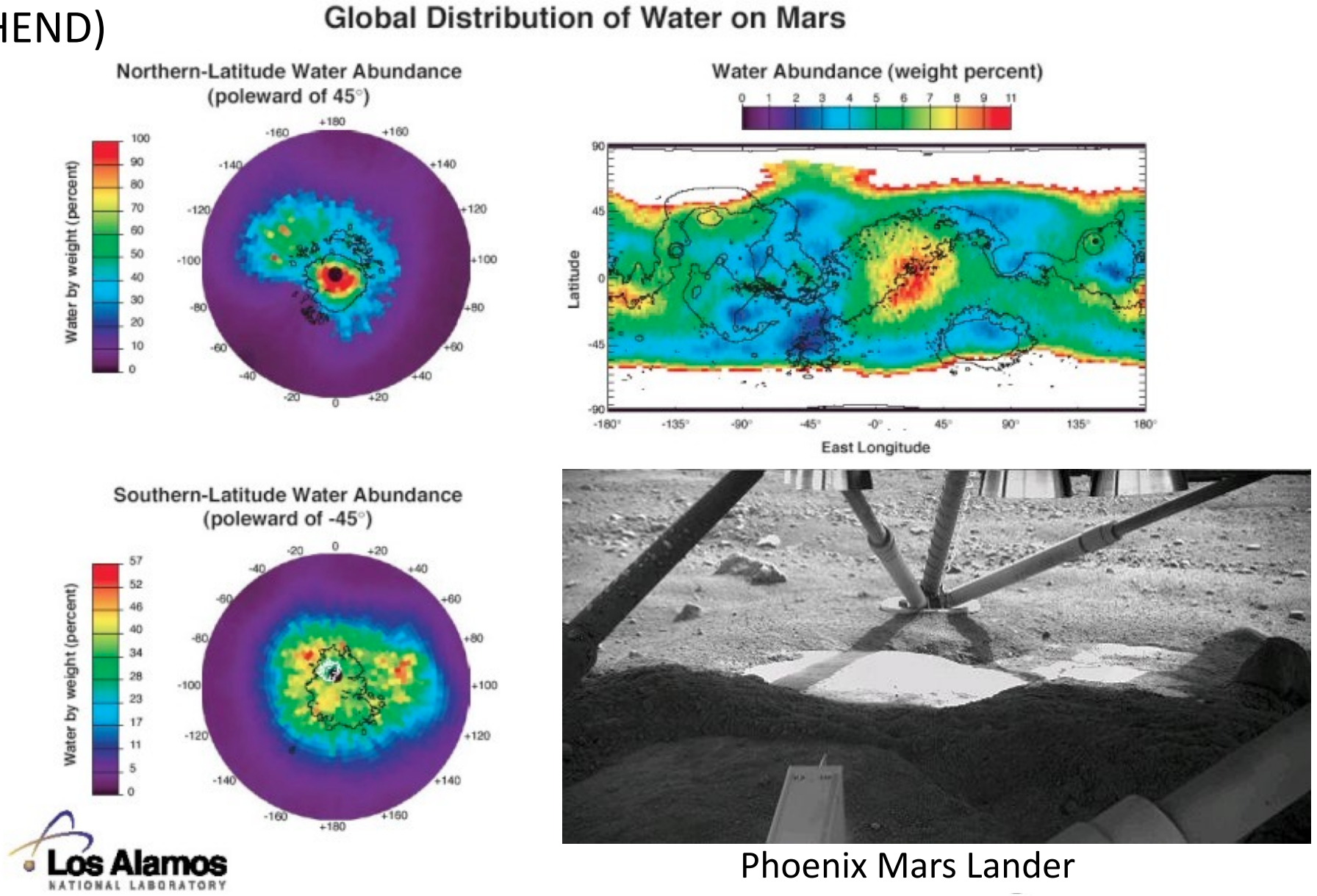

Phoenix Mars Lander

氷床の深さ

地表での水蒸気濃度の時間平均
　＝ある深さでの飽和水蒸気濃度の時間平均
でおおざっぱに決まるとされる

Schorghofer & Aharonson (2005)

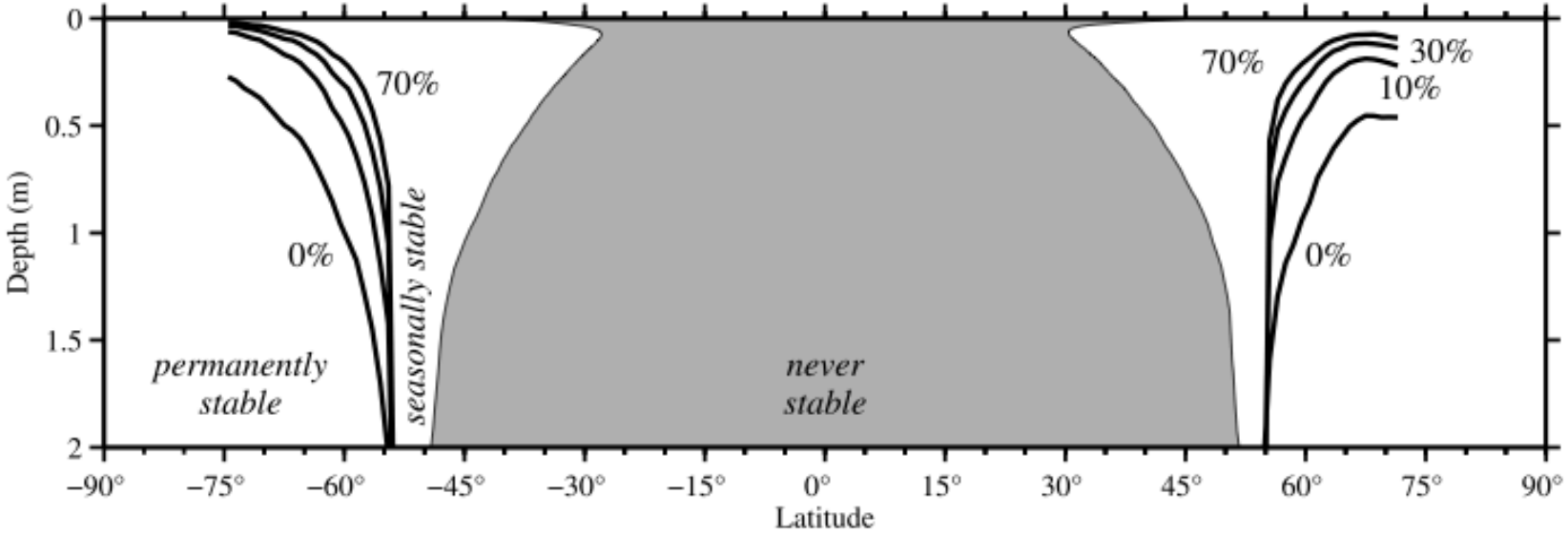

Figure 7. Permanent and seasonal stability for zonally averaged regolith parameters and humidities. The solid lines labeled "0%" indicate depths to permanent stability when no ice is present. When pore spaces are filled with ice at depths where it is stable, the burial depths become shallower than for dry regolith. Burial depths for 0%, 10%, 30%, and 70% volume fraction of ice are shown. No burial depths are plotted at the high latitudes where thermal inertias or humidities from TES are least reliable. In the presence of adsorption, free H_2O frost is not expected within the lightly shaded area at any day of the Mars year.

地下への水の拡散

Schorghofer & Aharonson (2005)

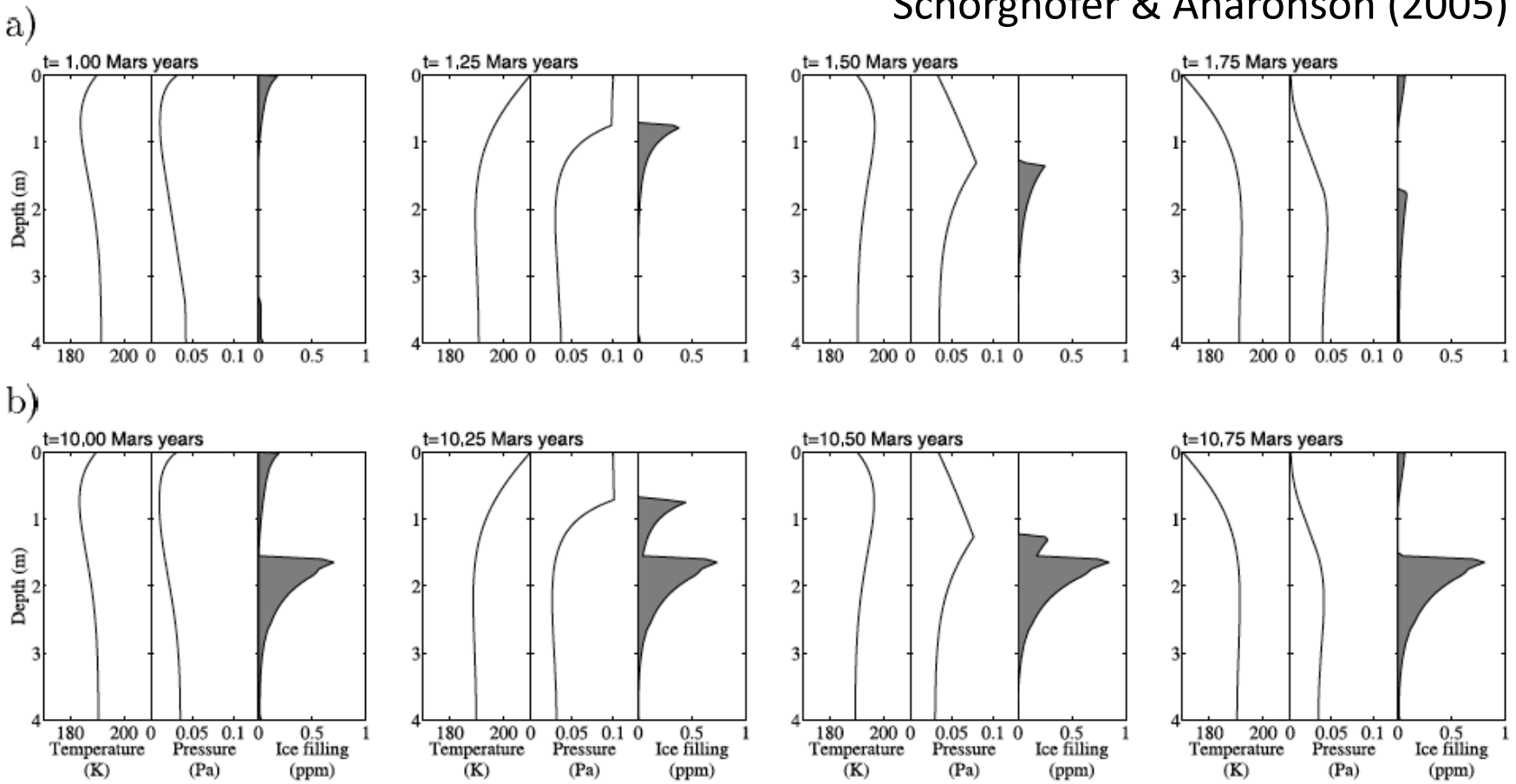

Figure 1. The downward migration of frost over two annual temperature cycles according to a one-dimensional model which simulates the conduction of heat and the diffusion, sublimation, and deposition of water vapor. Each panel shows instantaneous vertical profiles of temperature, partial pressure, and the fraction of pore space filled with ice. (a) The second year and (b) the tenth year after starting with an ice-free regolith. A layer of frost migrates inward during the warming part of the cycle and begins to fill the subsurface with ice. A sinusoidal surface temperature and constant daytime partial pressure are assumed in this model calculation. Model parameters: $p_0 = 0.1$ Pa, $D = 0.1(T/200\ \mathrm{K})^{3/2}\ \mathrm{cm^2 s^{-1}}$, $I = 280\ \mathrm{J\ m^{-2} K^{-1} s^{-1/2}}$, $\rho c = 1.28 \times 10^6\ \mathrm{J\ m^{-3} K^{-1}}$.

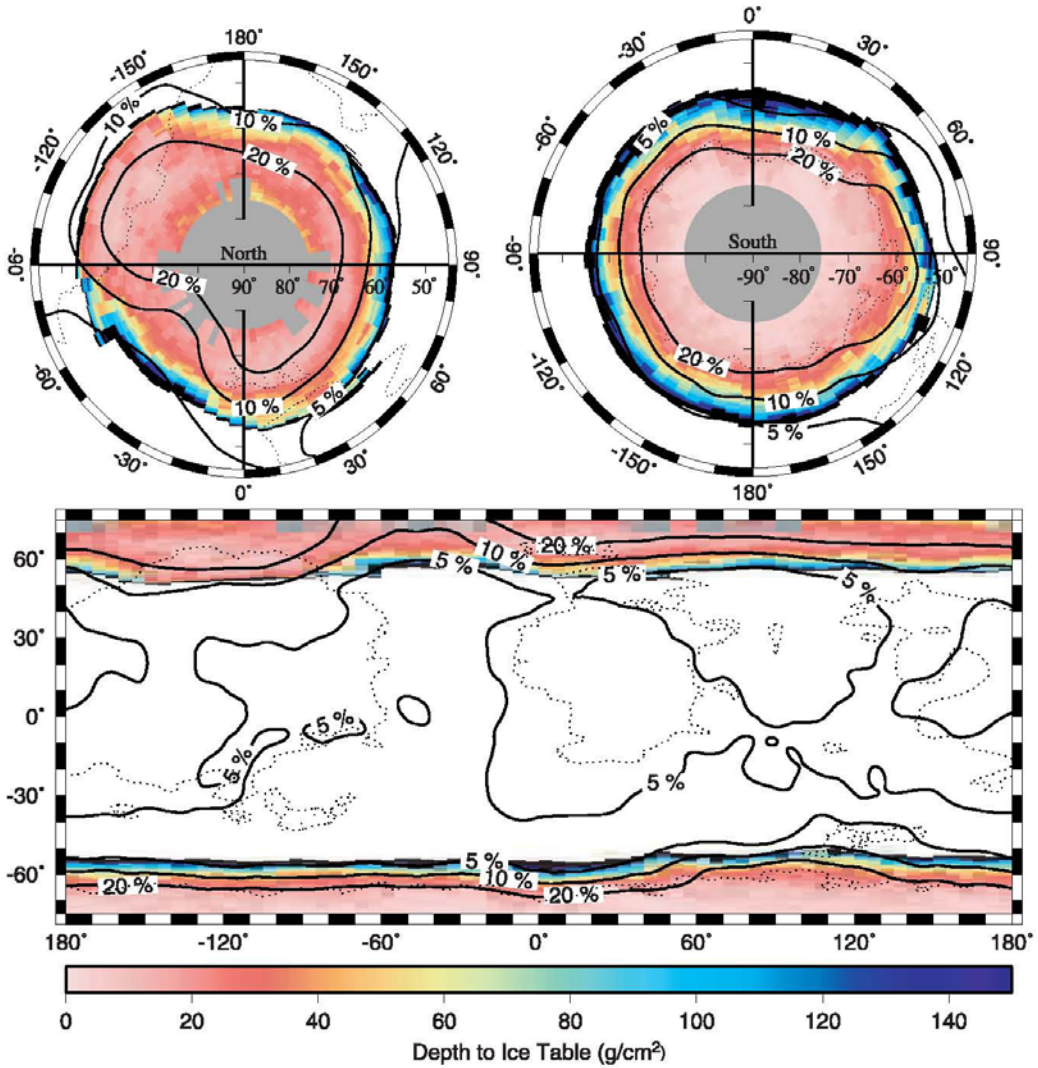

Figure 8. Color indicates depth to the ice table in g cm^{-2} when ice is in equilibrium with the atmospheric water vapor. Ground ice is unstable in the white area. Black segments indicate finite burial depths larger than 150 g cm^{-2}. Missing data points are shown in gray. Assumed volume fraction of ice is 40%, but the geographic boundary between icy and ice-free soil is independent of the ice fraction. Solid contours indicate water-equivalent hydrogen content in percent determined from neutron spectroscopy [*Feldman et al.*, 2004]. The dotted lines are 200 J $m^{-2}K^{-1}s^{-1/2}$ contours of thermal inertia.

Schorghofer and Aharonson (2005)

地下の氷層の分布

色： 大気中の水蒸気との平衡状態を仮定して計算される氷床までの深さ

実線： 中性子分光観測から見積もられた水含有量

→現在の気候とだいたい平衡状態か

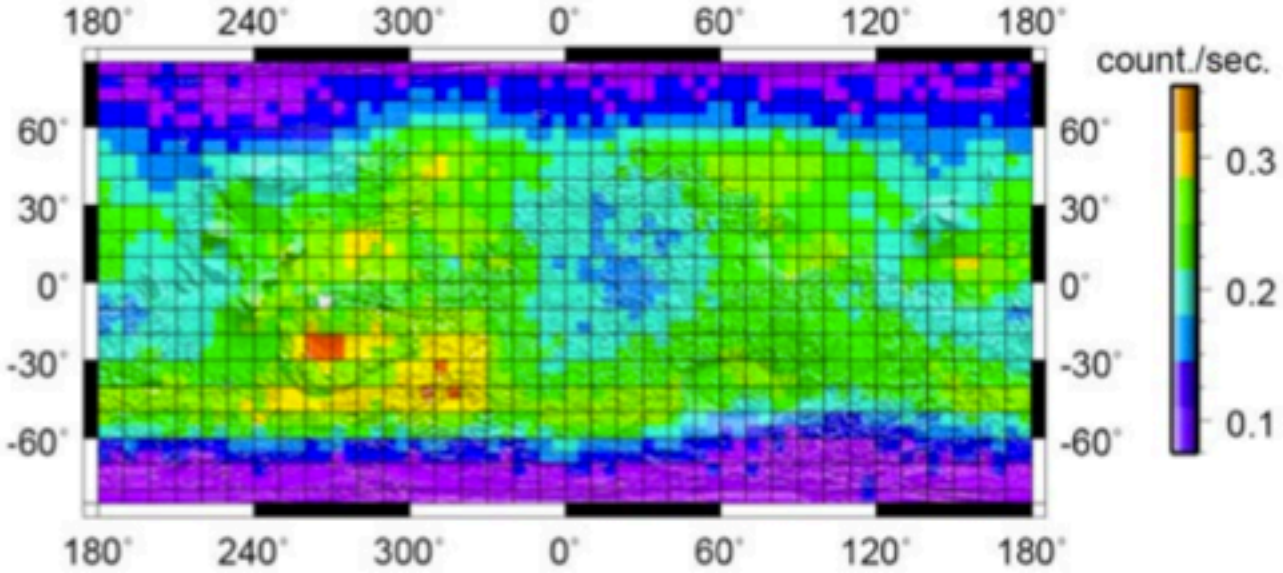

Surface distribution of albedo of epithermal neutrons (counts/sec) for summer seasons on Mars according to HEND data from Mars Odyssey

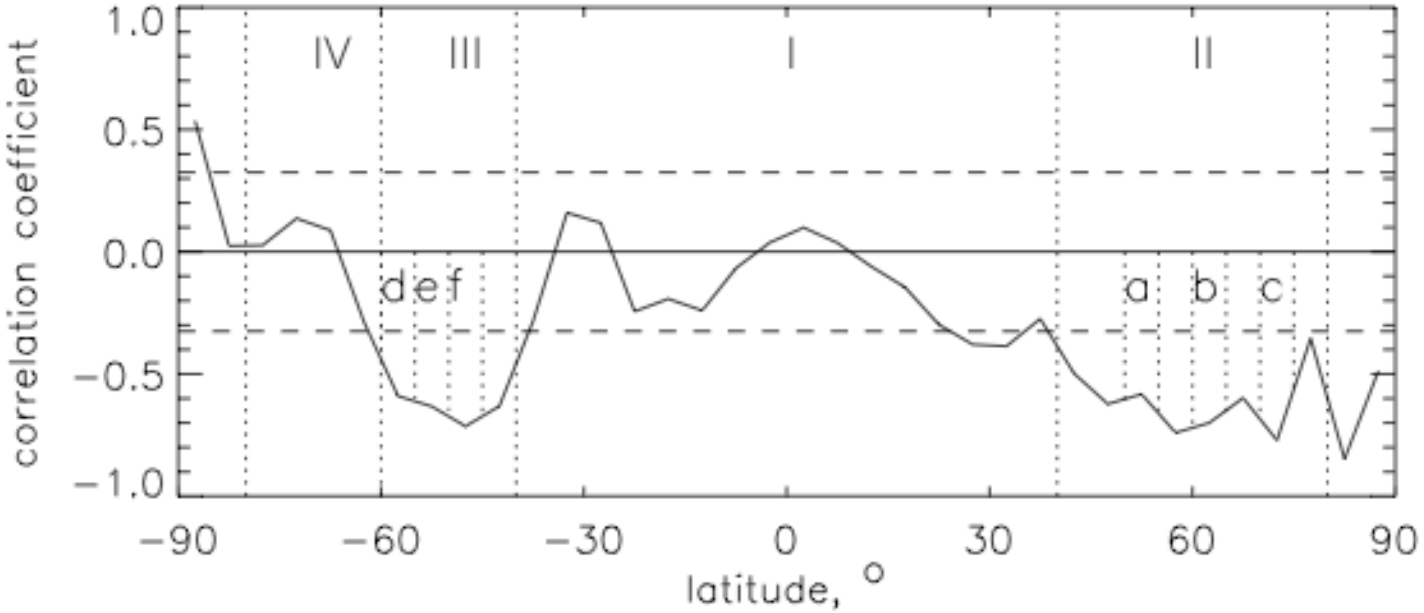

中性子アルベドと近赤外(1064nm)アルベドの緯度ごとの相互相関
（Mitrofanov et al. 2007）

地表の水:極冠

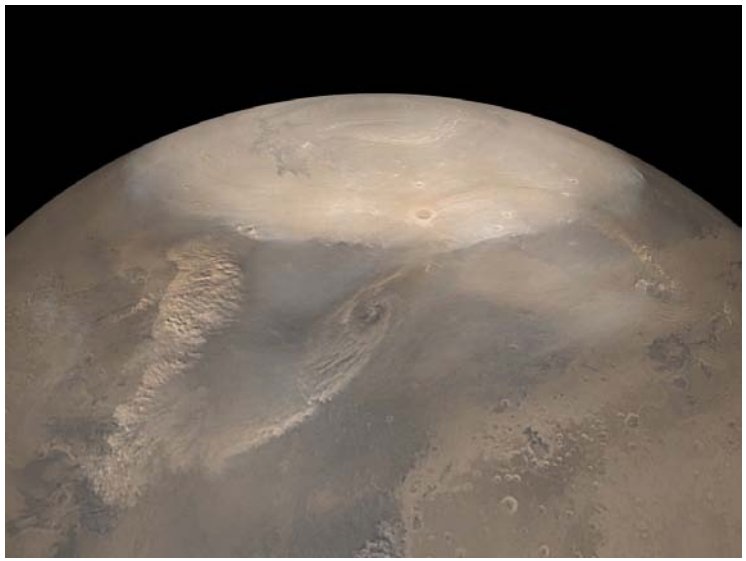

北極冠

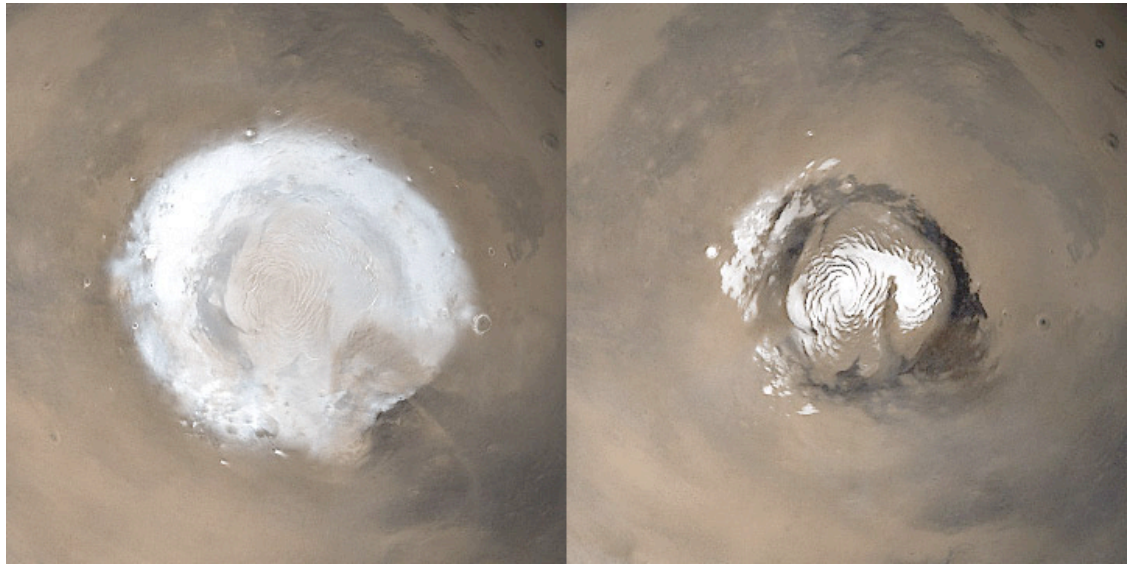

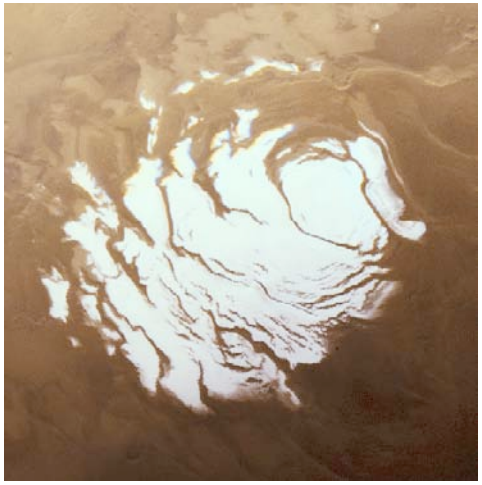

南極冠

H_2O氷＋CO_2氷

- 北極冠･南極冠とも、季節とともに拡大縮小
- 夏期も残る残存極冠
  - 北極ではH2O氷のみ
  - 南極ではH2O氷＋CO2氷
- 南極のCO2氷はH2Oのcold trap？

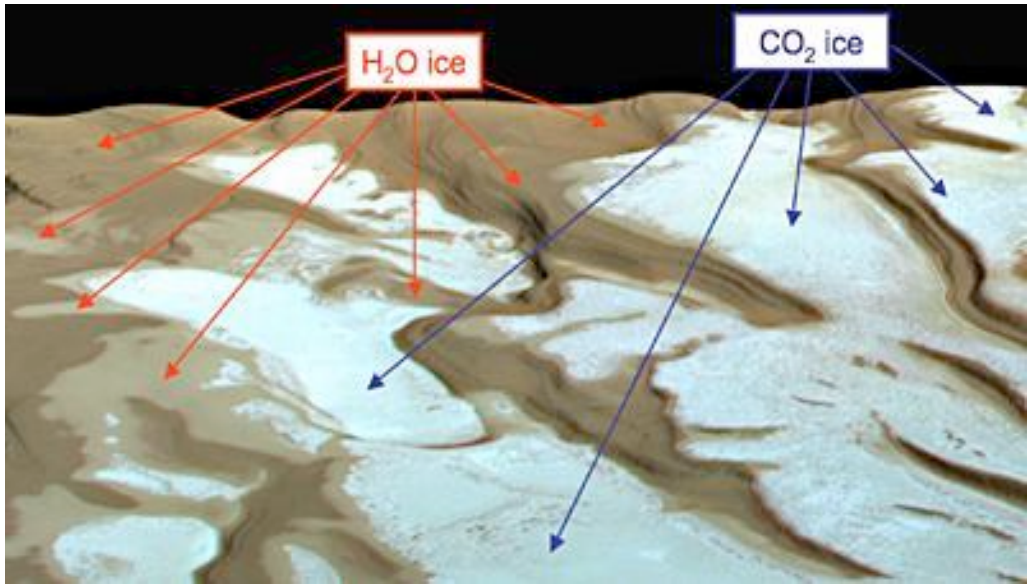

火星の季節

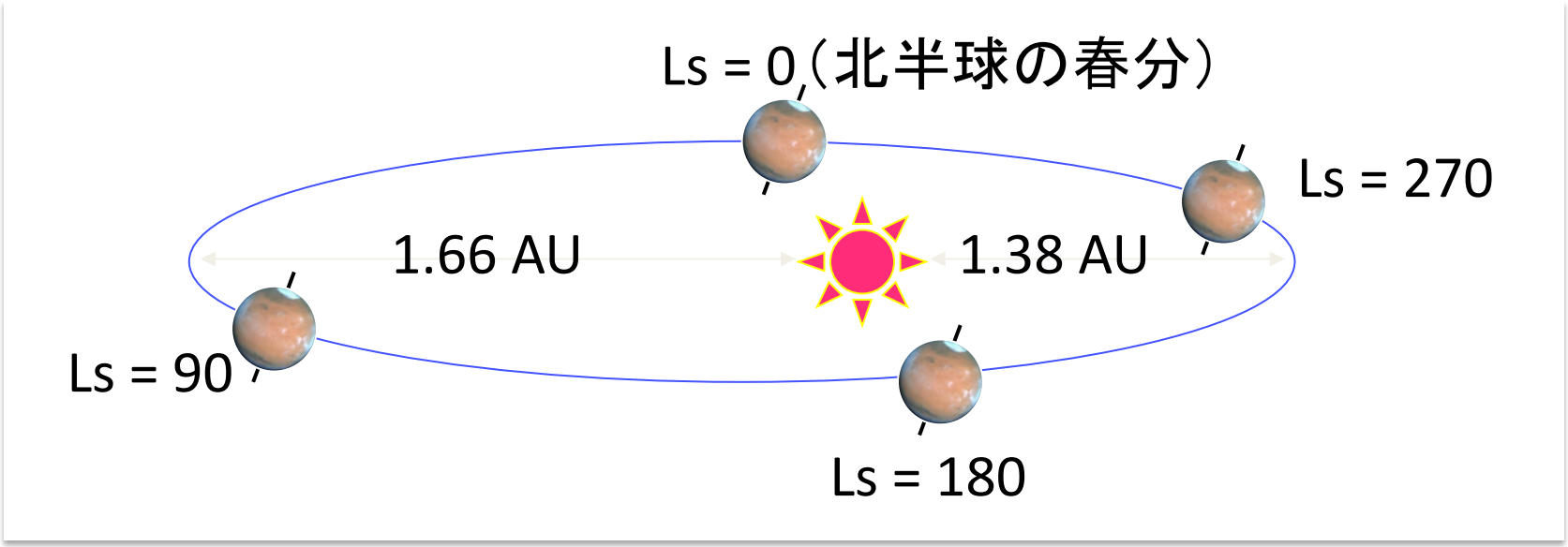

ダスト・雲・水蒸気の緯度分布の変動（MGS/TESによる）

ダスト

氷雲

水蒸気

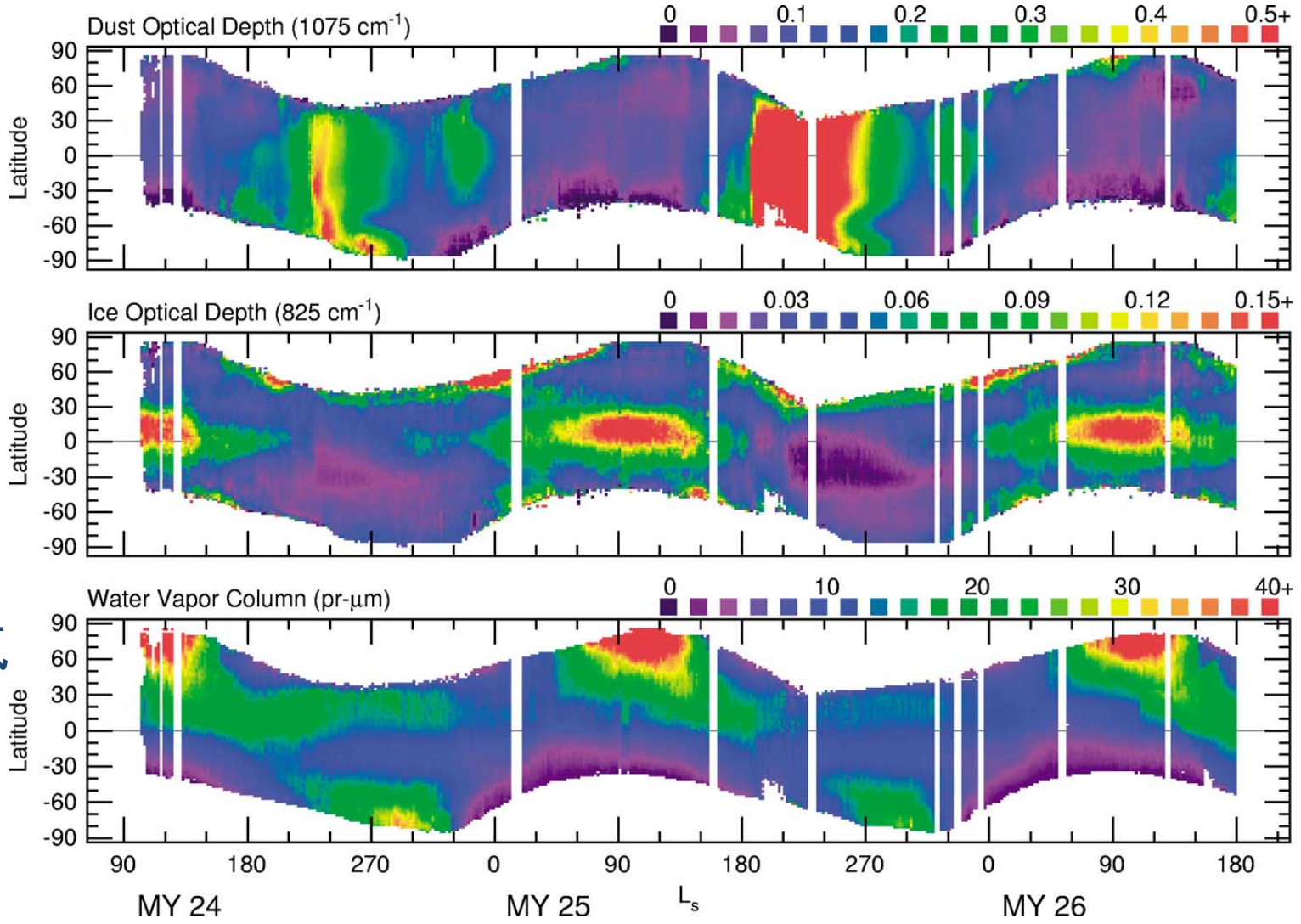

Smith, Icarus 167 (2004) 148–165

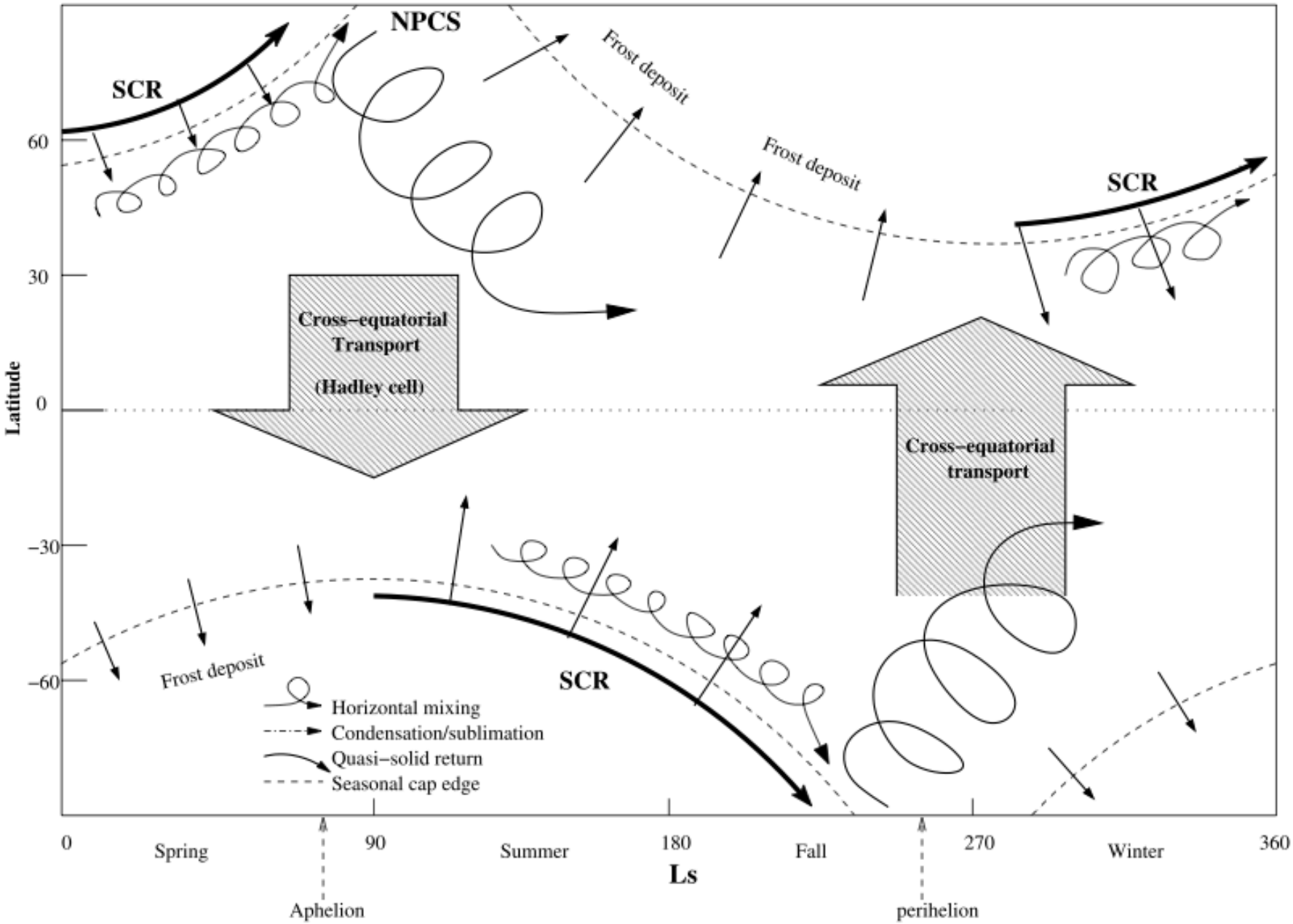

Figure 3. Chart describing the principal events affecting the Martian water cycle over the course of a year. NPCS stands for North Polar Cap Sublimation; SCR stands for Seasonal Cap Recession.

水蒸気の季節進行のイメージ

- 北極冠の消長が全体を駆動すると思われている。
- 北半球の春～夏に北極冠が昇華して北極域の水蒸気濃度が上昇、これが(この時期の弱い)水平渦で低緯度に拡散的に運ばれる。
- 低緯度に運ばれた水蒸気の一部は赤道越えのハドレー循環で南半球に運ばれる。
- 北半球の秋～冬には北極冠で凝結により水蒸気濃度が低下し、南北濃度勾配が逆転するため、傾圧不安定などに伴う水平渦で低緯度から北極域に水蒸気が拡散的に戻る。南北濃度勾配を決める低緯度の水蒸気量は、それまでの水蒸気輸送の履歴で決まる。

地下氷・土壌吸着水の効果

- これを考慮すると水蒸気量が20%増加（Richardson & Wilson, 2002：GCM＋2層レゴリスモデル）
- これを考慮すると水蒸気量が1/2～1/4に減少（Böttger et al., 2005：GCM＋10層レゴリスモデル）

- 水蒸気の出入りを直接的にとらえた観測はない
- いずれにせよ長い時間スケールでの水循環にとっては重要である可能性が高そう

ハドレー循環による雲形成

- 地形の非対称と近日点位相の効果で凝結高度に違い
- 1年間の積算では北極域に水を集める傾向

H2O雲

濃淡は水蒸気混合比

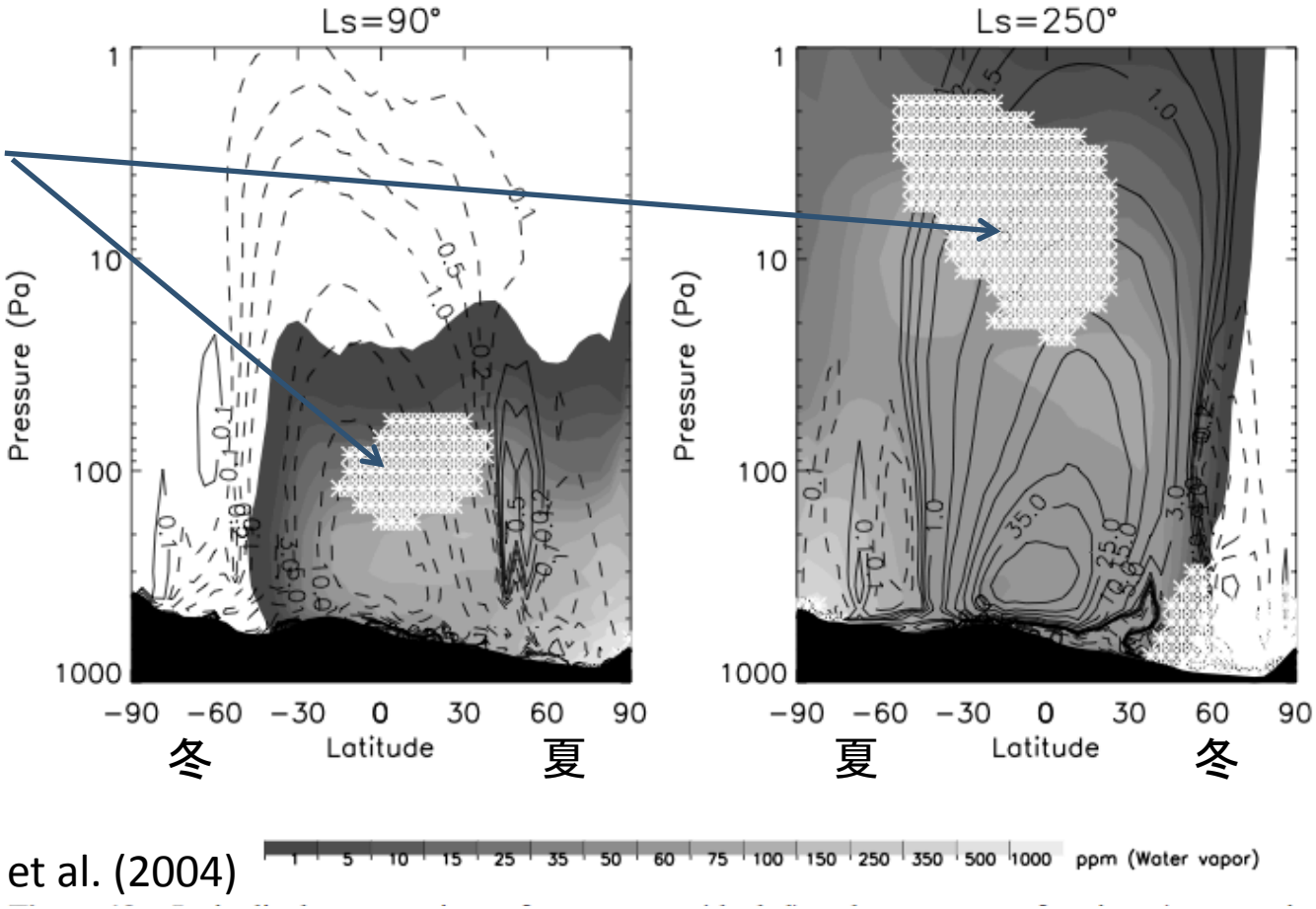

Montmessin et al. (2004)

Buried glaciers

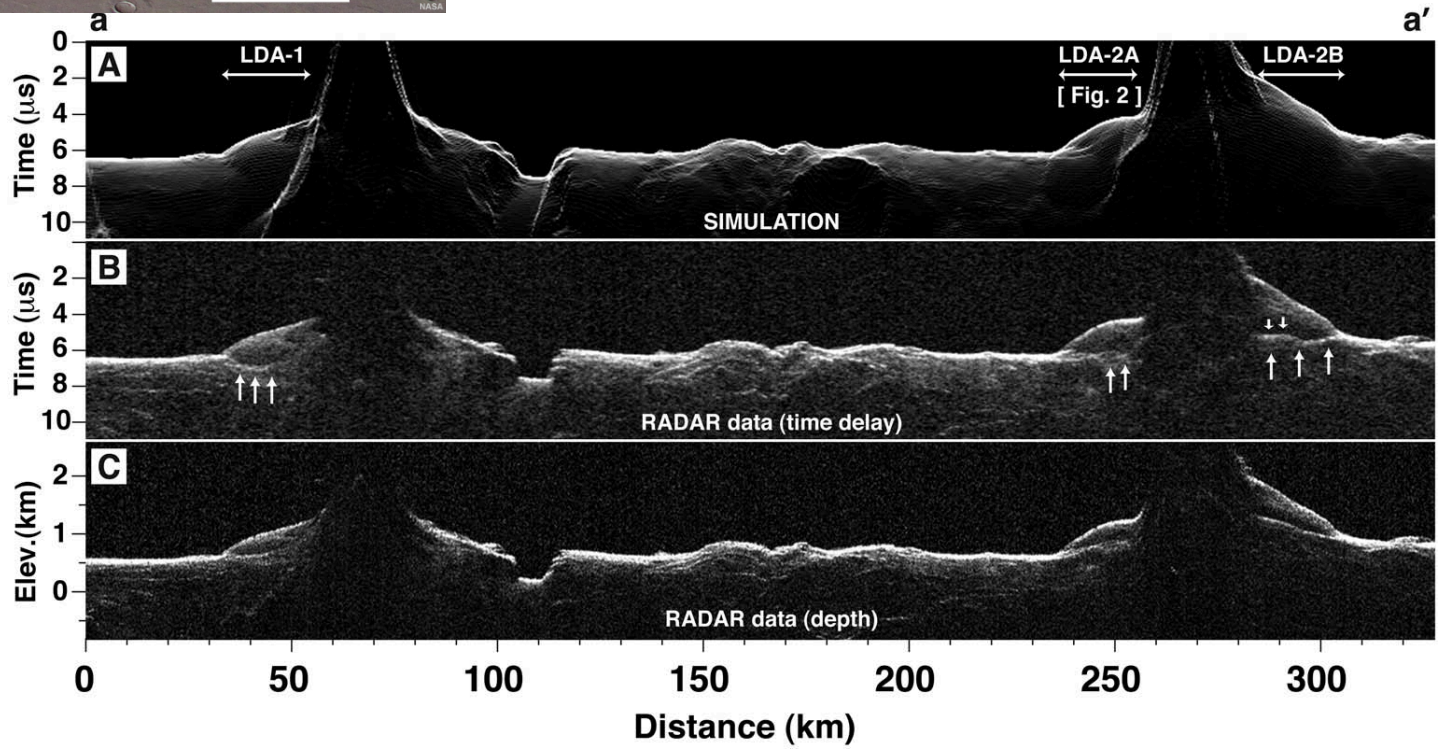

Gullies

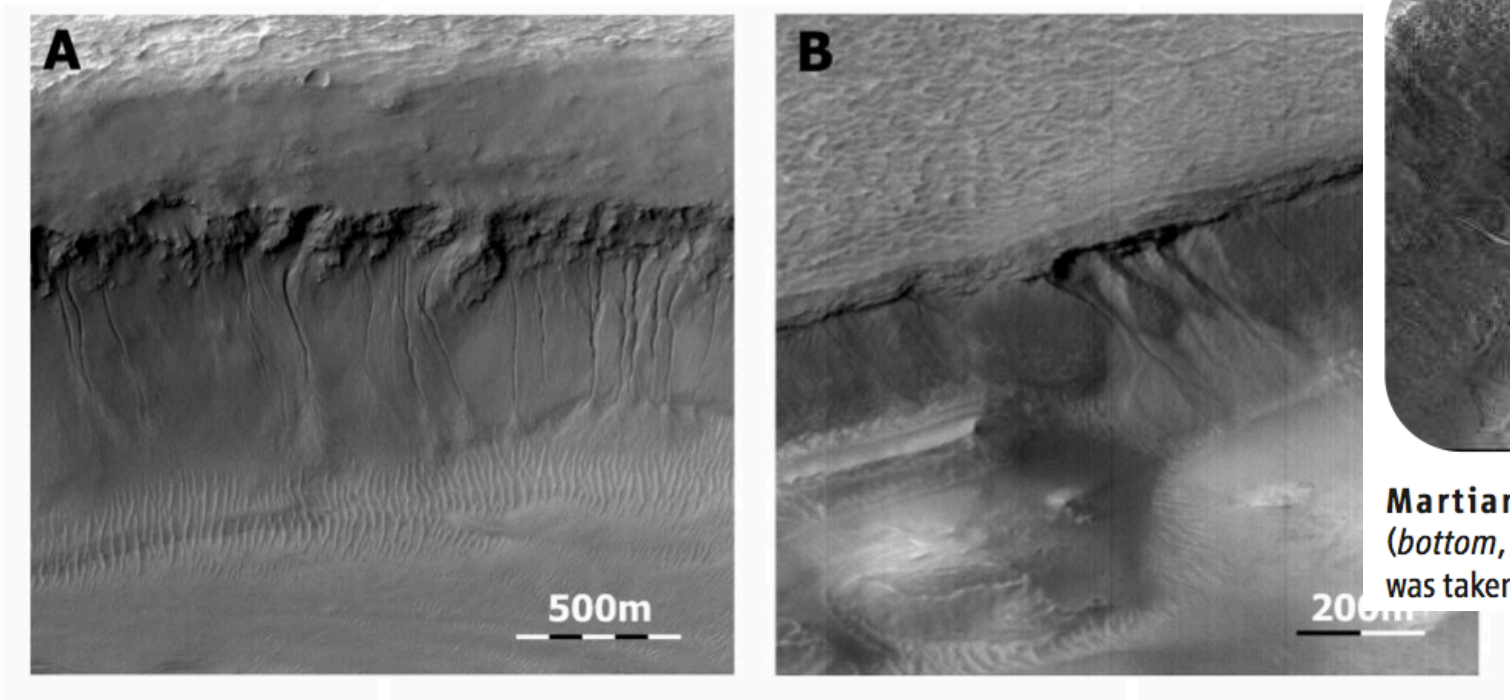

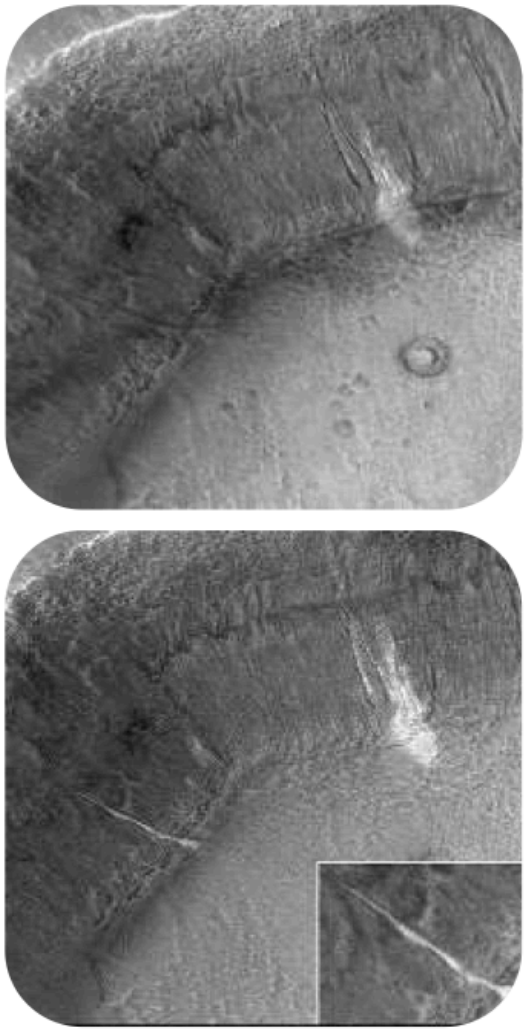

Martian weeping. New deposit (*bottom, left*) formed since top image was taken may be water-borne debris.

Figure 1. Images of gullies on Mars: (a) on the wall of Nirgal Vallis near 29.7°S × 39°W, subframe of Mars Orbiter Camera (MOC) image M03-02290, and (b) in a valley in Gorgonum Chaos near 38.5°S × 171.5°W, subframe of MOC image M07-02909. Gully features frequently appear to stem from or below cohesive strata exposed along the slope.

自転軸傾斜角と軌道離心率の変動、およびそれらがもたらす極域の日射変動

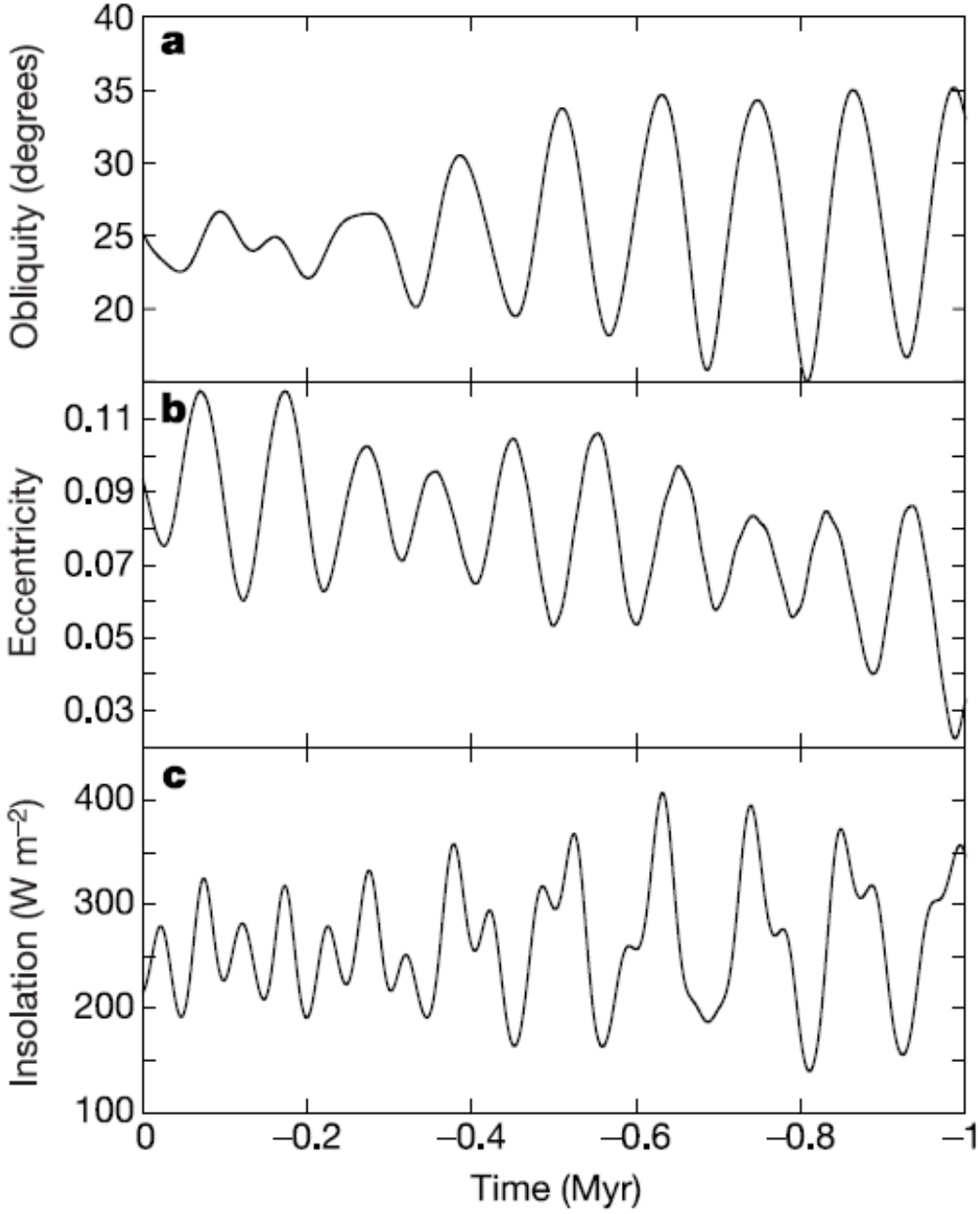

Laskar et al. (2002)

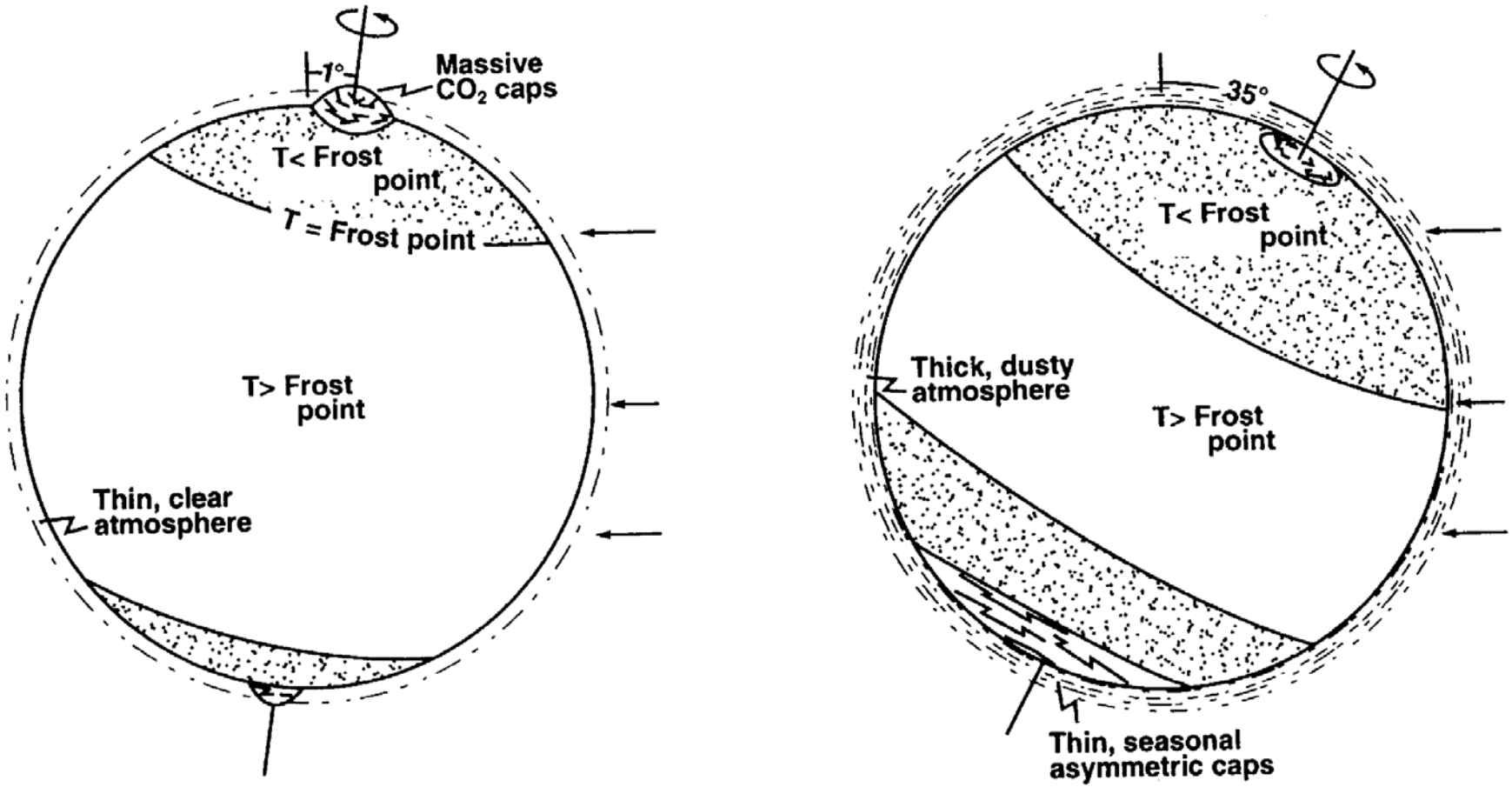

- 自転傾斜角が小さい→極域が寒冷化→水蒸気が極域に凝結（夏にもCO2氷に覆われて蒸発しない）→水蒸気濃度低下
- 自転傾斜角が大きい→極域が温暖化→水蒸気が極域から蒸発→水蒸気濃度上昇

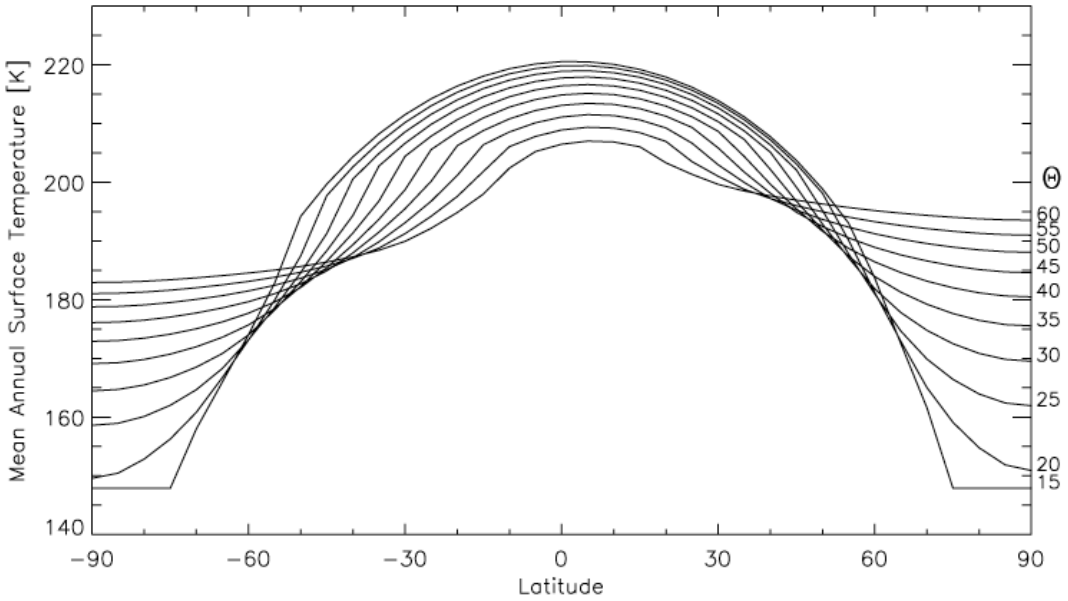

Figure 3. Mean annual surface temperature for a range of obliquities. The eccentricity is 0.12, and the L_S at which perihelion occurs is 270, corresponding to southern summer. A thermal inertia of 250 J m^{-2} s$^{-1/2}$ K^{-1}, an albedo of 0.25, a surface pressure of 600 Pa, and an infrared dust opacity of 0.1 are assumed. Discontinuities in the slope of each curve are due to the effects of seasonal CO_2 frost.

Mellon & Phillips (2001)

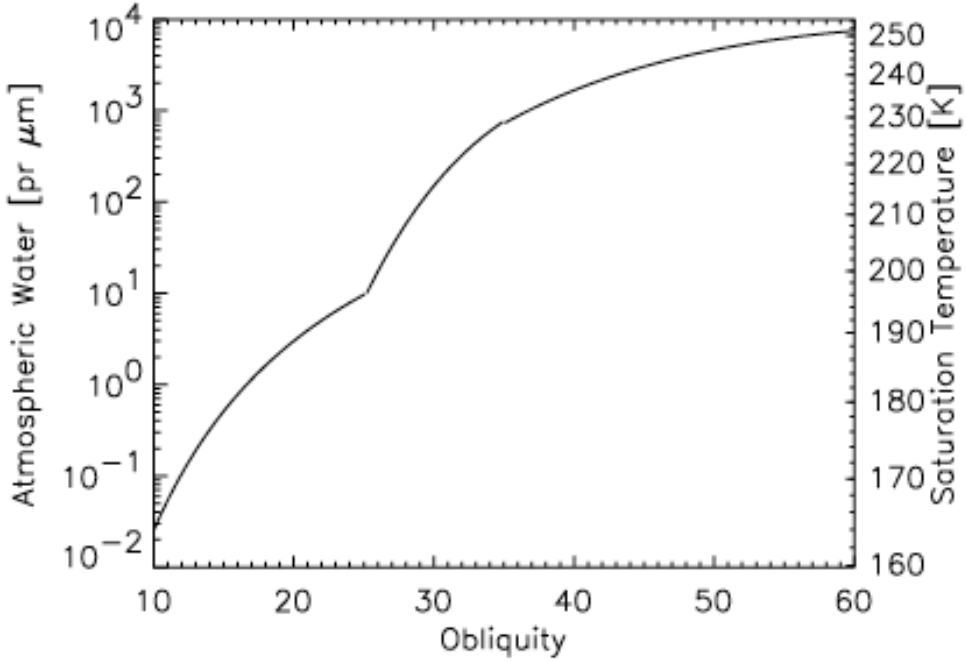

Figure 4. Average atmospheric water column abundance and

Characteristic time (Kieffer and Zent, 1992)

- Response times (Years)
  - CO_2 cap stabilization of atmospheric pressure 100
  - Stabilization of an H_2O cap 0.1-100 Myr
  - Dust deposition of polar lamina (30 m) 100,000
  - Regolith (100 m) 10,000
  - Regolith (1 km) 1 Myr
- Driving functions
  - Precession of the equinox 175,000
  - Oscillation of eccentricity 100,000 and 2 Myr
  - Variation of obliquity 125,000 and 1.3 Myr

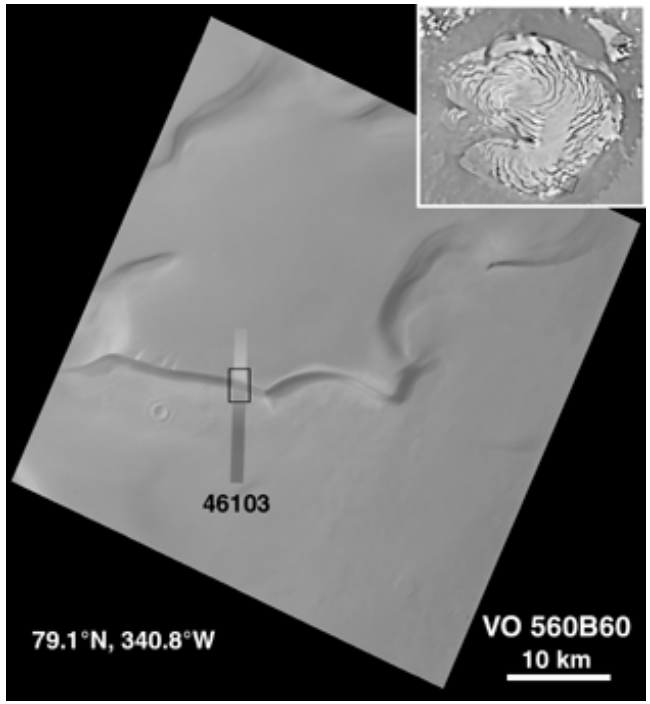

極冠堆積物

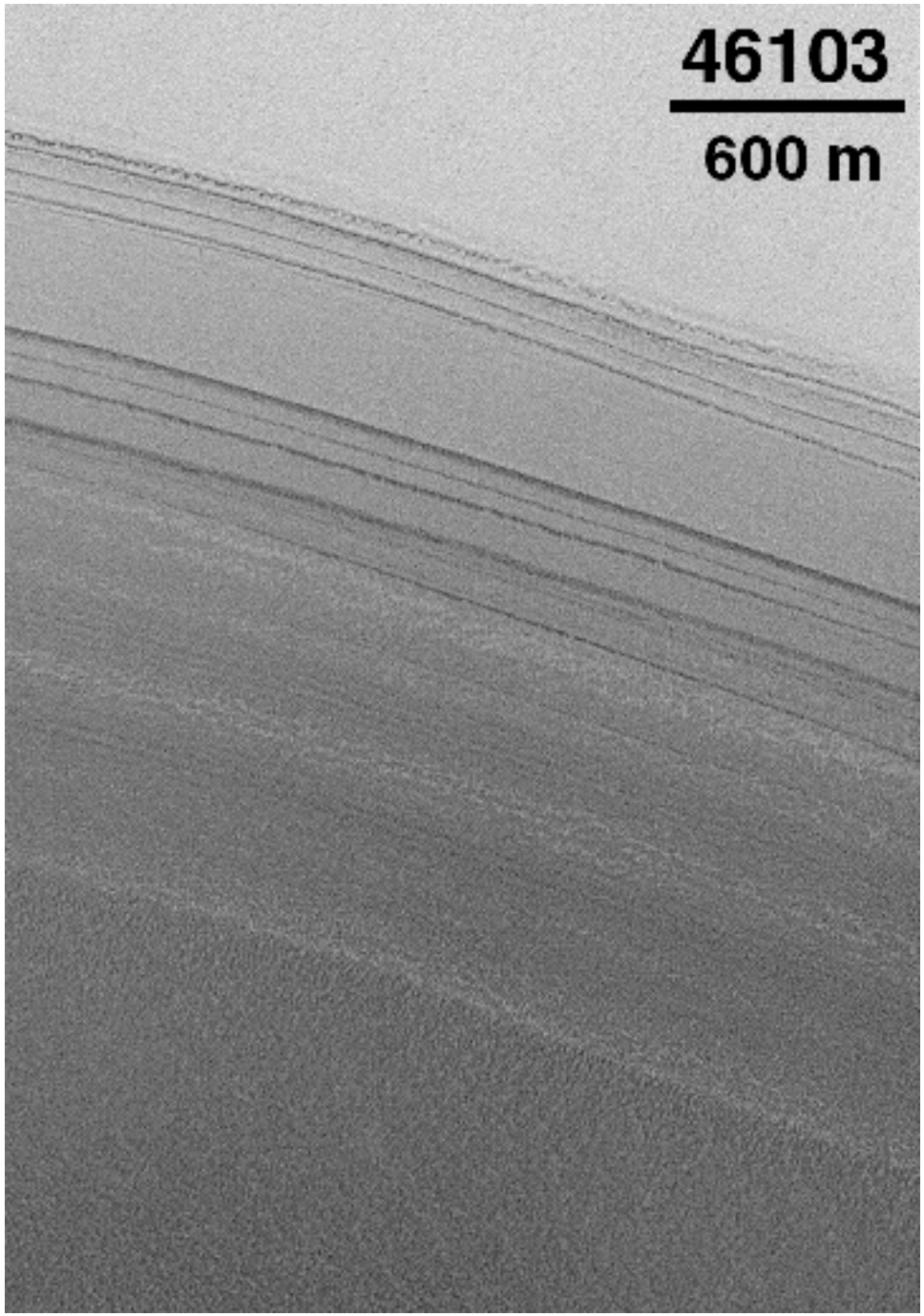

過去数百万年の氷床の変動
Schorghofer (2007)

- ある時期に低緯度まで雪が降り積もって氷床が形成されたとして、そこからスタート
- 大気中の水蒸気量と地表温度の変化を外部から強制として与える
- 最初の氷床がそのまま残っている成分(ice sheet)と、いったん蒸発して大気中の水蒸気となったあと再び地下に拡散で戻ってきた成分(pore ice)を区別

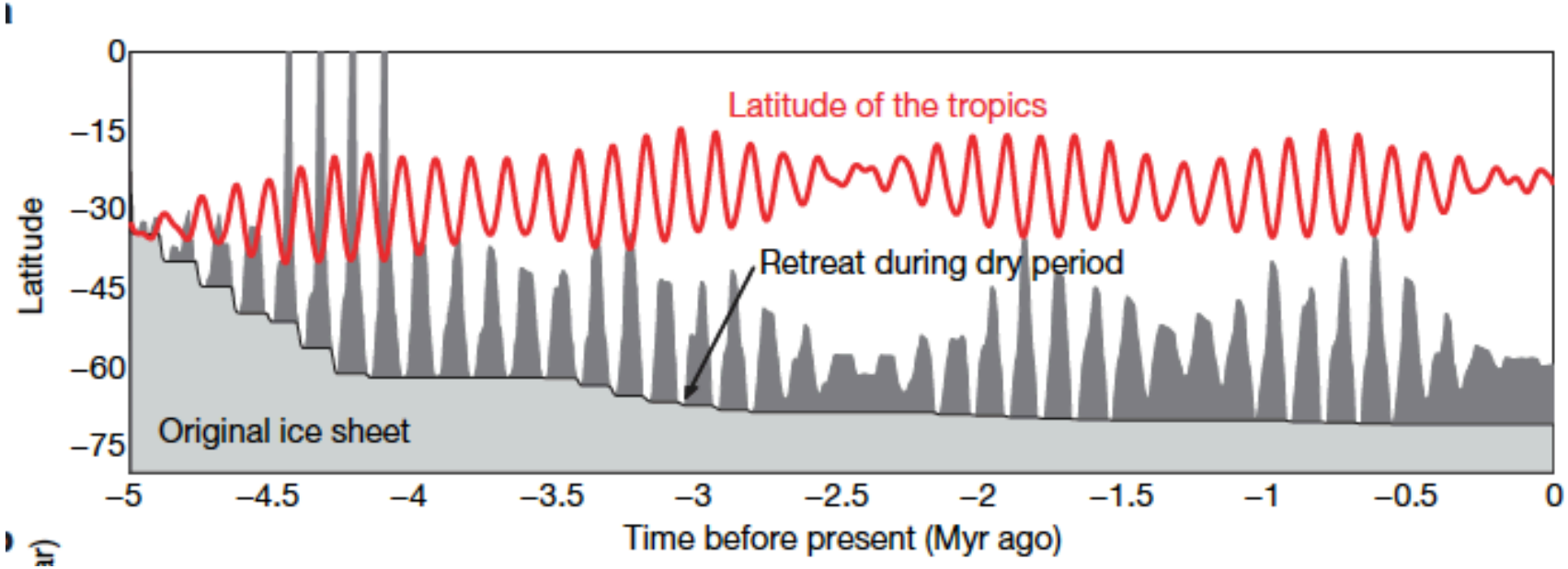

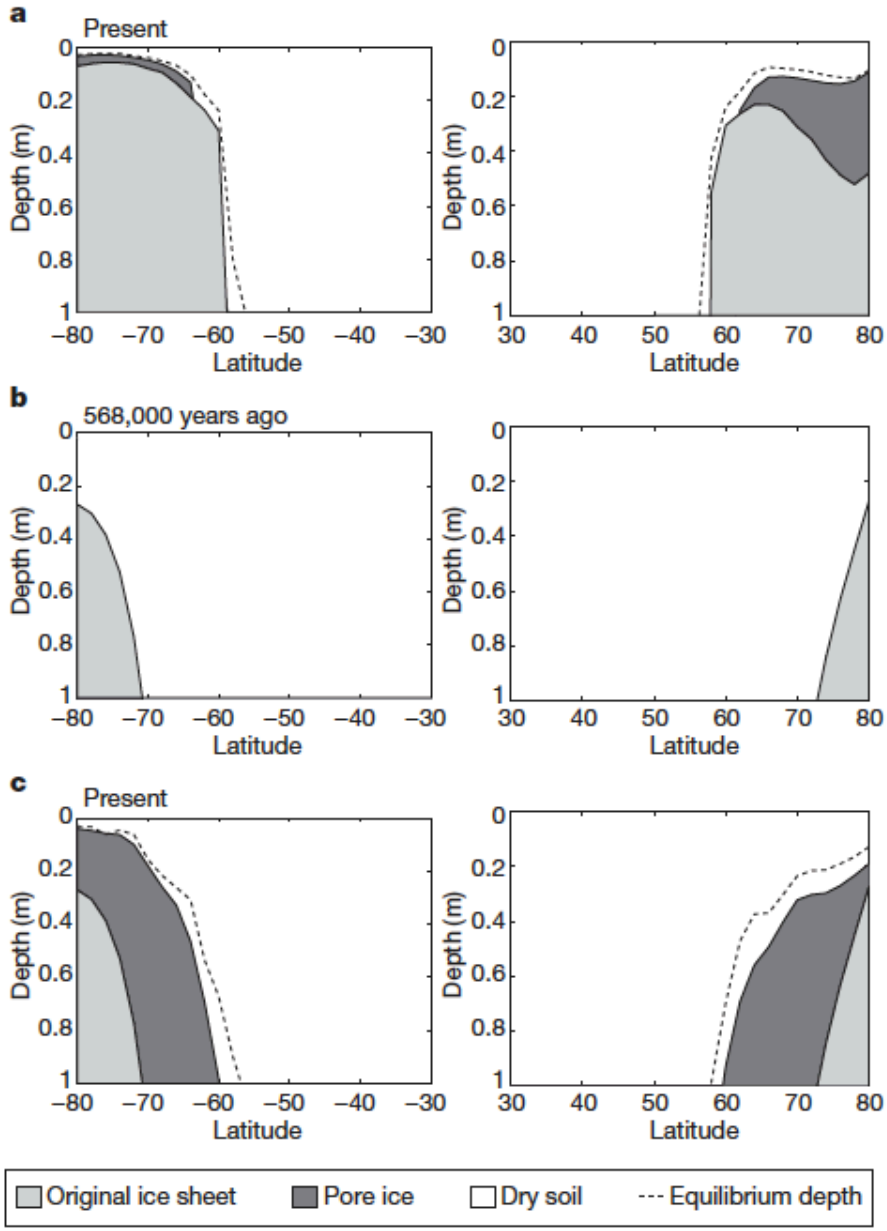

Figure 1 | Snapshots of the vertical ice distribution from model calculations. **a**, At present and with atmospheric humidity constant throughout history. **b**, For strongly varying atmospheric humidity, 568,000 years ago. **c**, For strongly varying atmospheric humidity, at present. Dashed lines show the present-day equilibrium depth.

水蒸気濃度を変化させなかった場合の現在の地下氷分布

水蒸気濃度を変化させた場合の最近の自転角傾斜角極小時

水蒸気濃度を変化させた場合の現在の地下氷分布

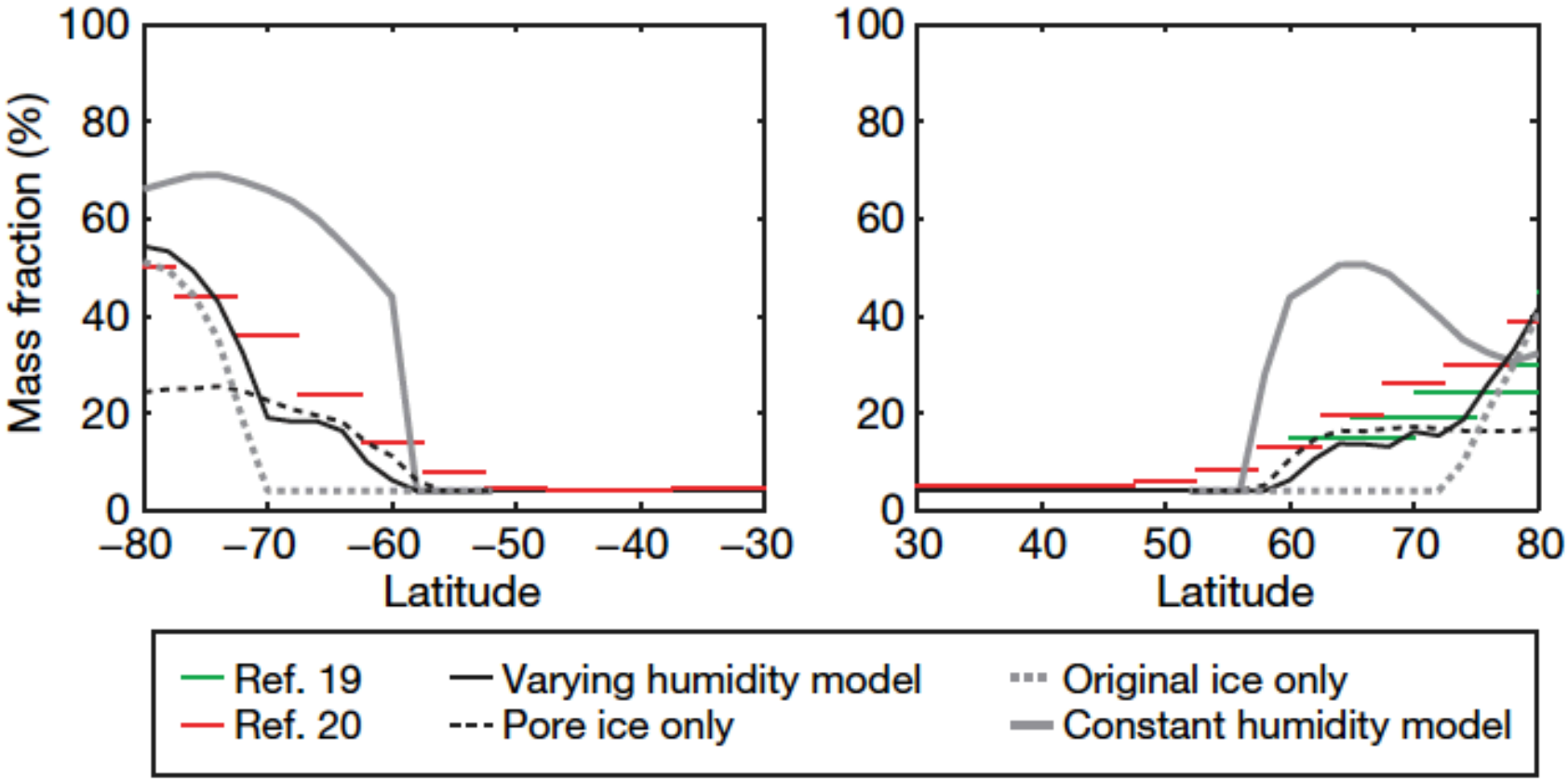

Figure 3 | Comparison with measurements by GRS onboard Mars Odyssey. Coloured bars show the ice (mass) fraction according to refs 19 and 20, in latitude bins, zonally averaged and assuming a homogeneous vertical distribution of hydrogen. The solid black and grey lines show the fraction of ice in the topmost metre of the soil according to the model described in the text and shown in Fig. 1a and c. The dry component is assumed to contain 4% water-equivalent hydrogen. The dashed and dotted lines pertain to the varying humidity scenario.

南極冠のCO2残存極冠

青いところにCO2氷　　青いところにH2O氷

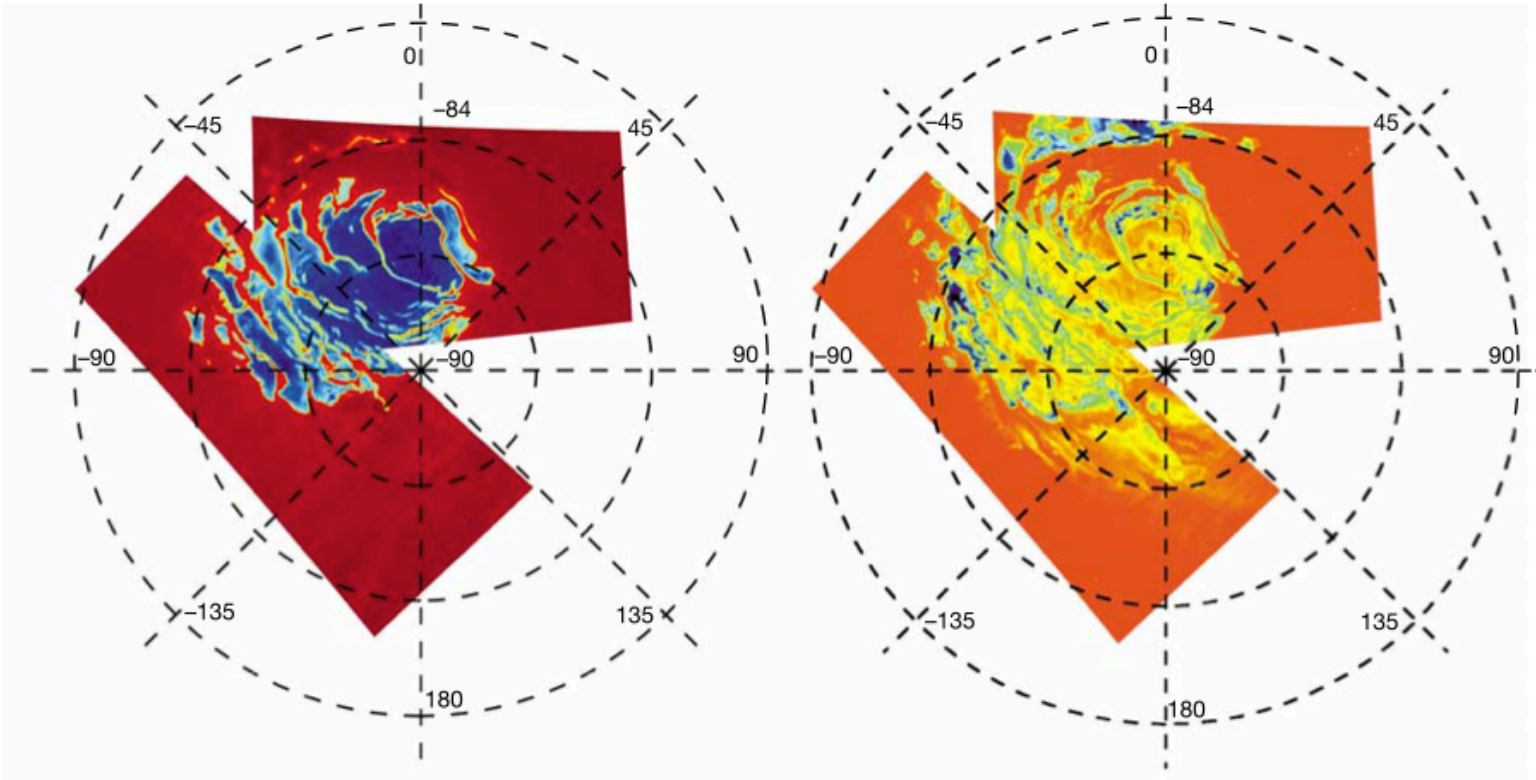

Figure 1 Global maps of CO_2 and H_2O ices at the south pole of Mars. Left, the CO_2-ice absorption feature is scaled from blue (deep) to brown (CO_2-ice-free areas); right, mapping of the H_2O ice, from blue (deep absorption) to red (ice-free). Comparison shows that the H_2O-ice areas extend far beyond the CO_2-rich bright cap, along its scarps up to isolated units tens of kilometres wide.

Bibring et al. (2004)

CO2残存極冠のおかげで
残存H2O氷も存在？

- Water in the southern polar cap : remnant from the past where the southern water ice was stable?
- How stable is the current southern water ice cap?

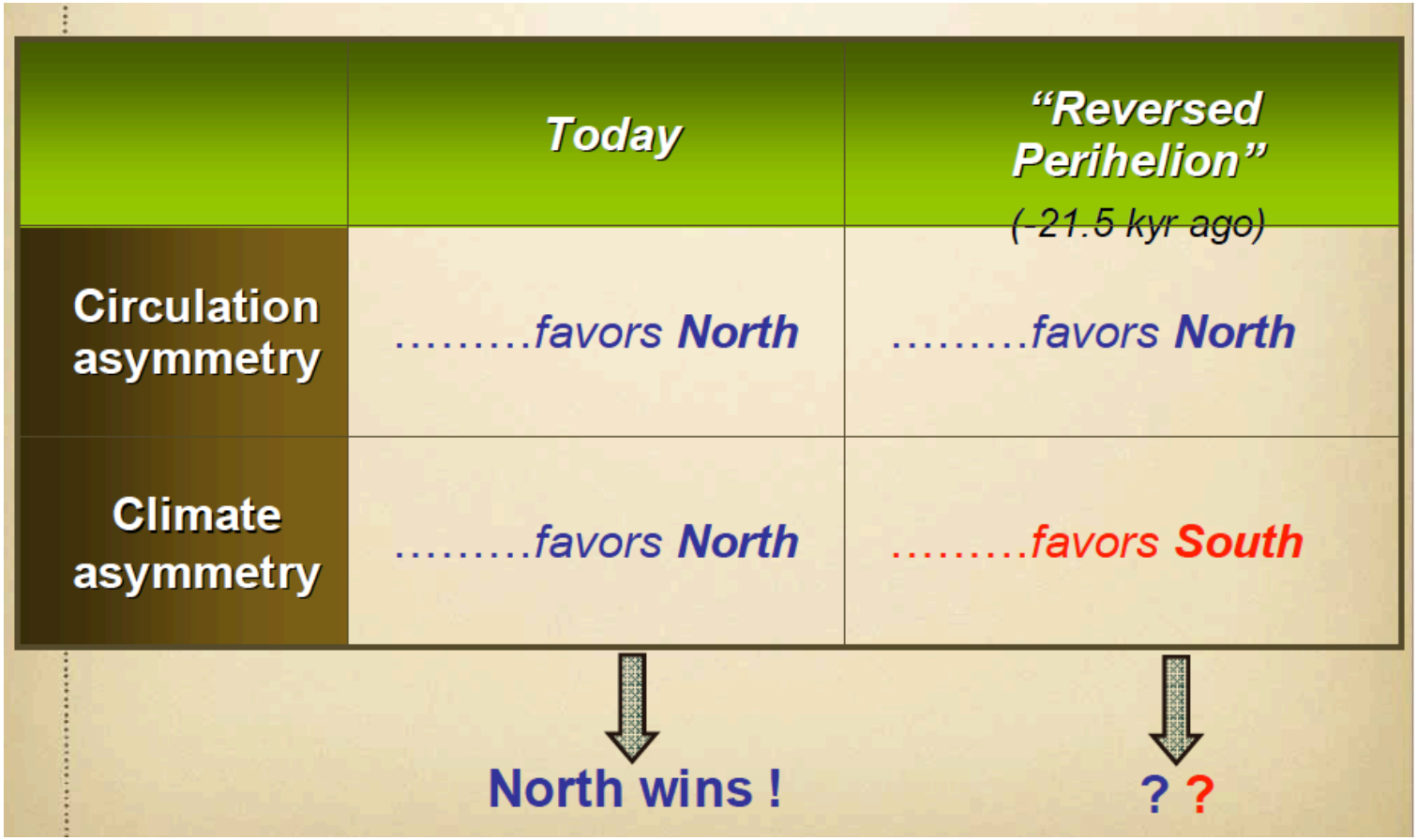

Montmessin et al. (2007)

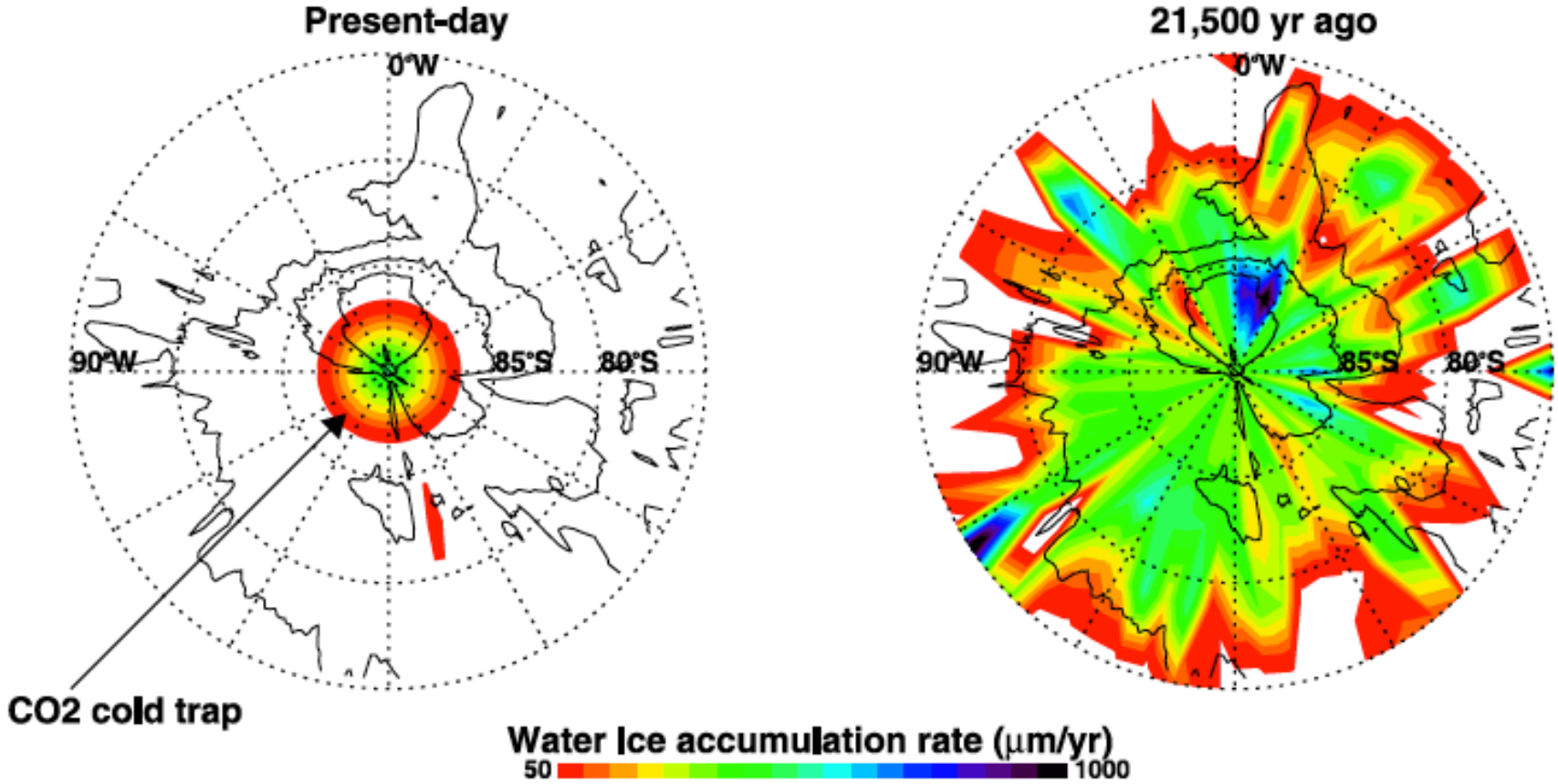

Figure 5. A comparison of water ice accumulation rates predicted by the model in the south polar region for the two perihelion configurations. Present-day map shows net accumulation only at the south pole itself (equivalent to 1 grid point in the model) where the prescription of a CO_2 cold trap forces a local and permanent deposition of water ice. In the reversed perihelion simulation (Figure 5, right), the CO_2 cold trap has been removed and the pattern of accumulation is only controlled by a precipitation versus sublimation positive balance on an annual average.

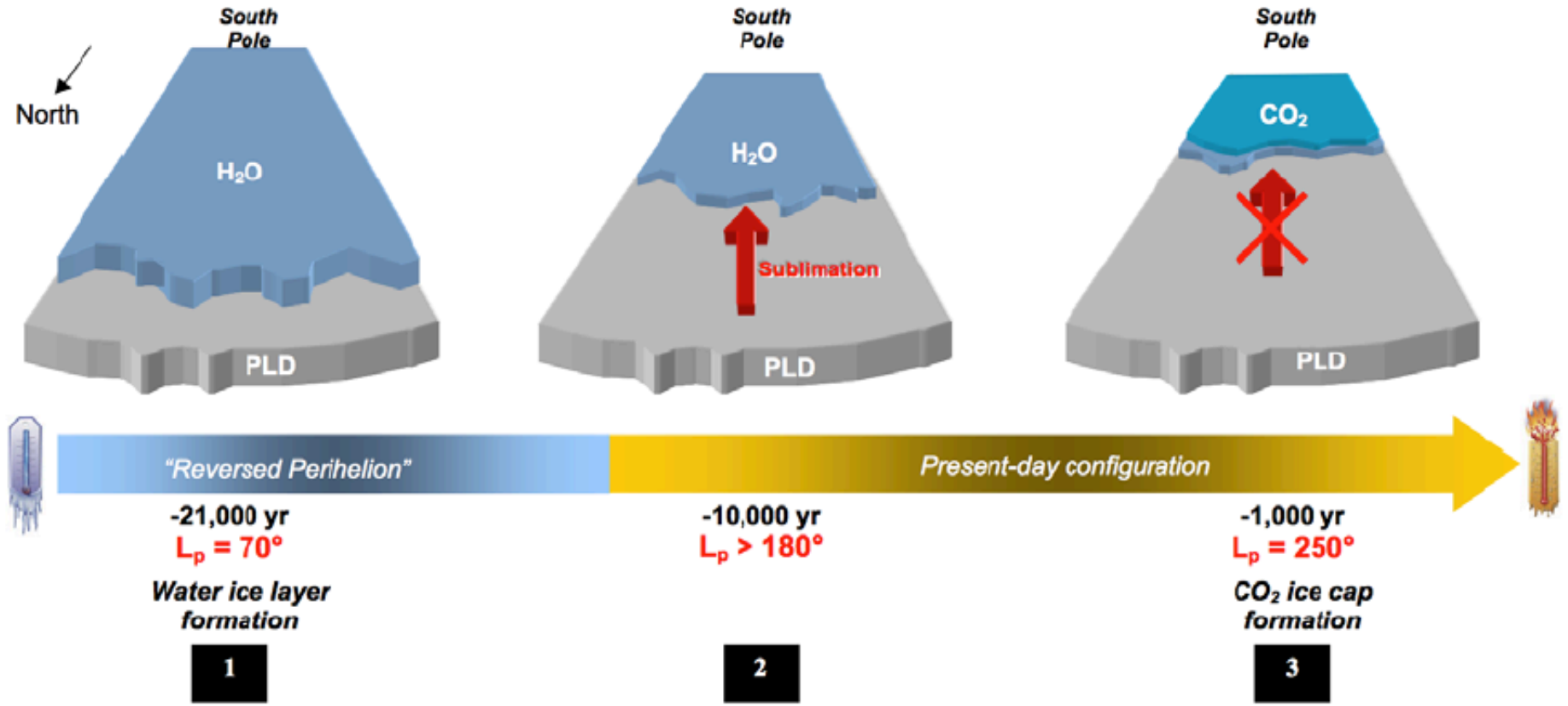

Figure 9. Illustration summarizing the sequence of events in the south polar region since the last reversed perihelion regime of the precession cycle. At event 1 time, water was extracted off the north polar cap and was deposited over the south PLD terrains thanks to a favorable summer insolation gradient between the poles. For event 2, passage to present-day configuration, with perihelion argument now entering a northern spring regime, reversed the orientation of the insolation gradient and forced water to progressively return back to the north pole. For event 3, in a third act, the erosion process stopped as permanent CO_2 ice slabs formed and kept water from subliming further.

浸食されつつある残存CO2極冠

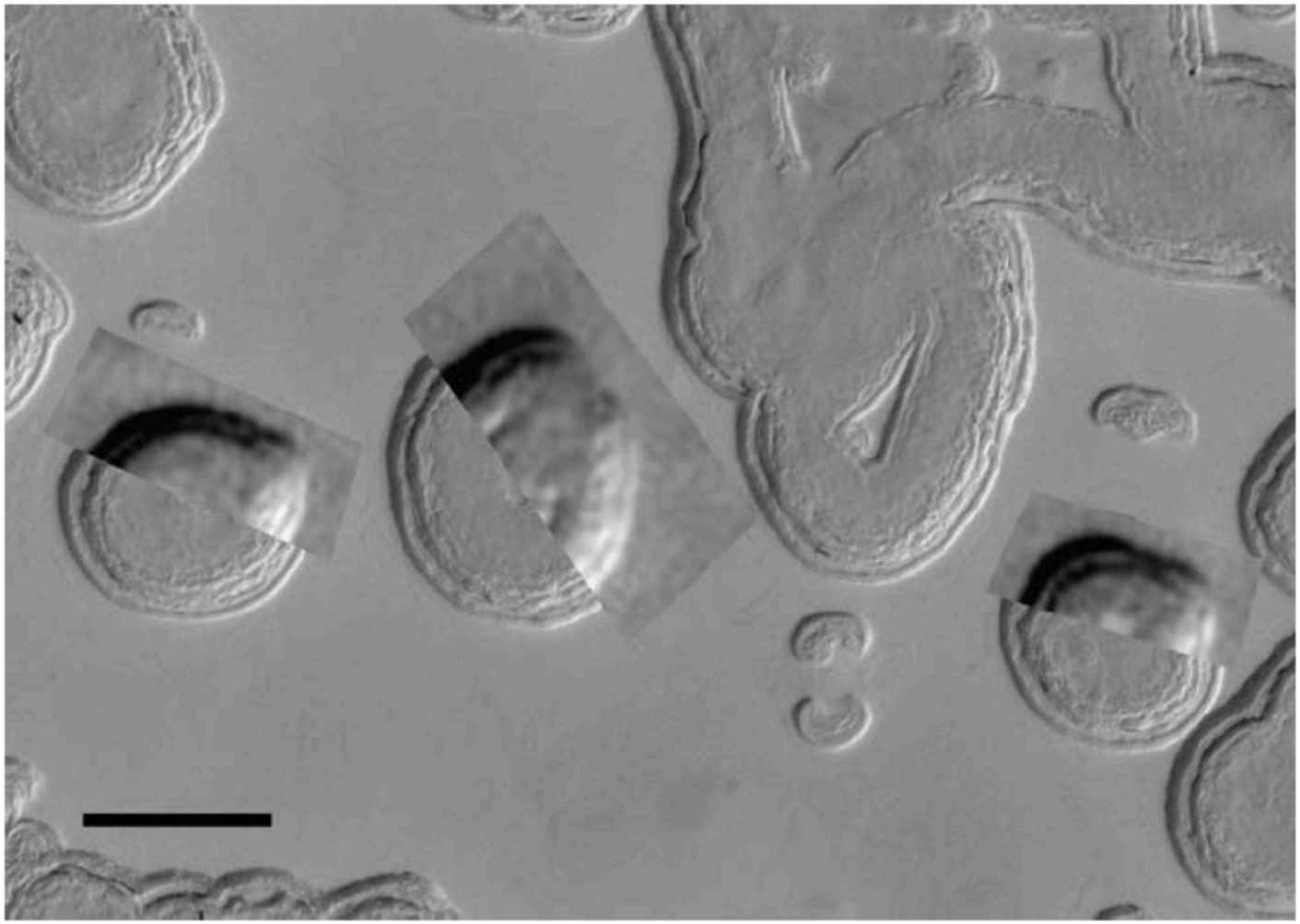

Fig. 8. Three year changes in unit B. Registered clips from MOC image E11-01220 superposed on HiRISE image PSP_004744_0870. Note that the three year change includes one or two ridges interior to the present depression edge. Illumination in MOC images from upper left, in HiRISE more from the left. MOC $L_s = 286°$, HiRISE $L_s = 287°$. Scale bar 50 m. Centered at 86.9°S, 89.4°W.

7. Down

Debri
wasting
initially
Fig. 5E–C
"downw
these ma
by some
in other
material
mesas of
of rough,
to the sc
are show
the typic
trated sc
and late
than doe
outlines
interpret
occurren

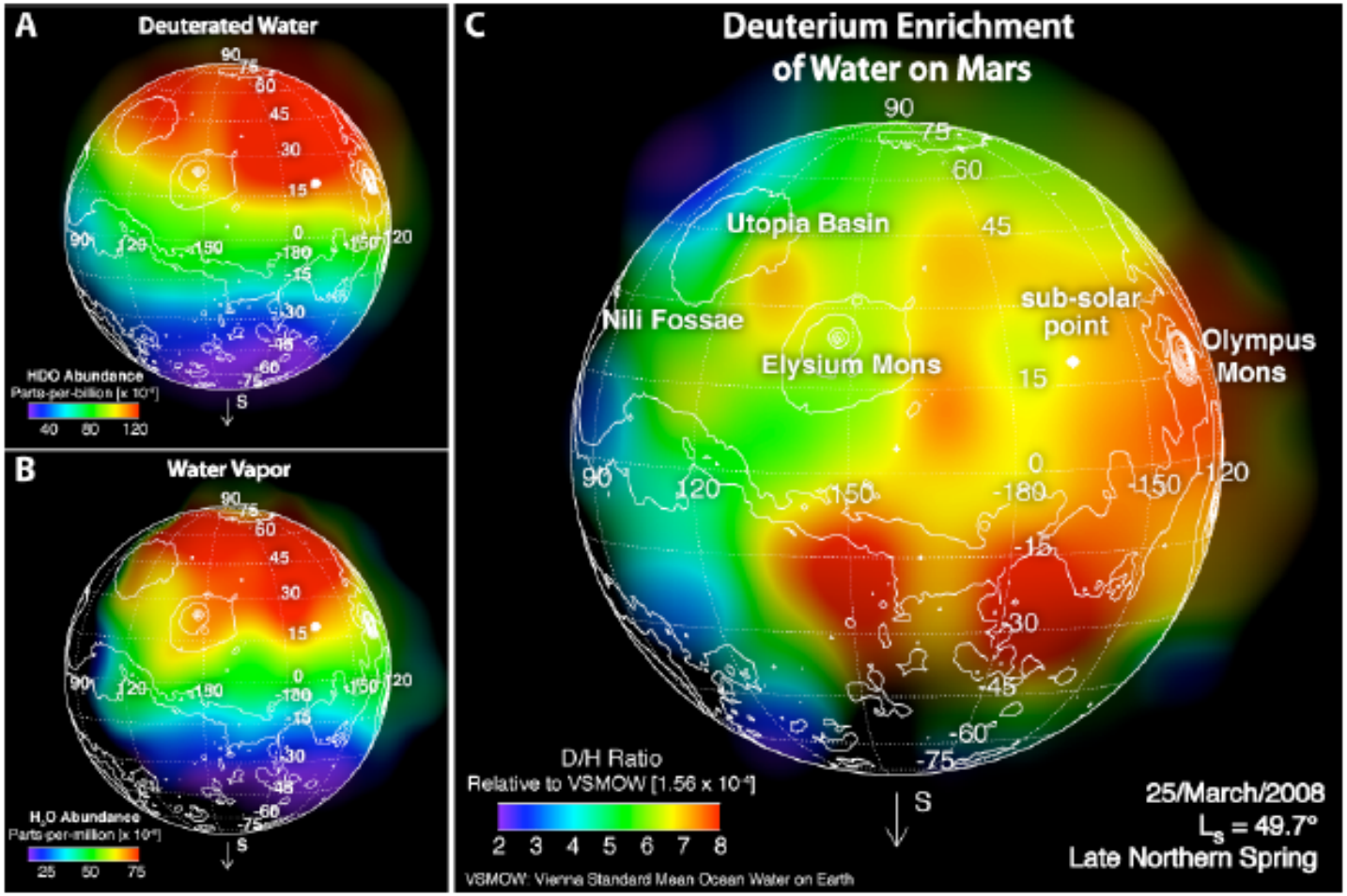

Mapping the D/H of water on Mars using high-resolution spectroscopy

Geronimo L. Villanueva[1,2], M. J. Mumma[1], R. E. Novak[3], T. Hewagama[1,4], B. P. Bonev[1,2], M. D. DiSanti[1]

Fractionation in atmospheric circulation

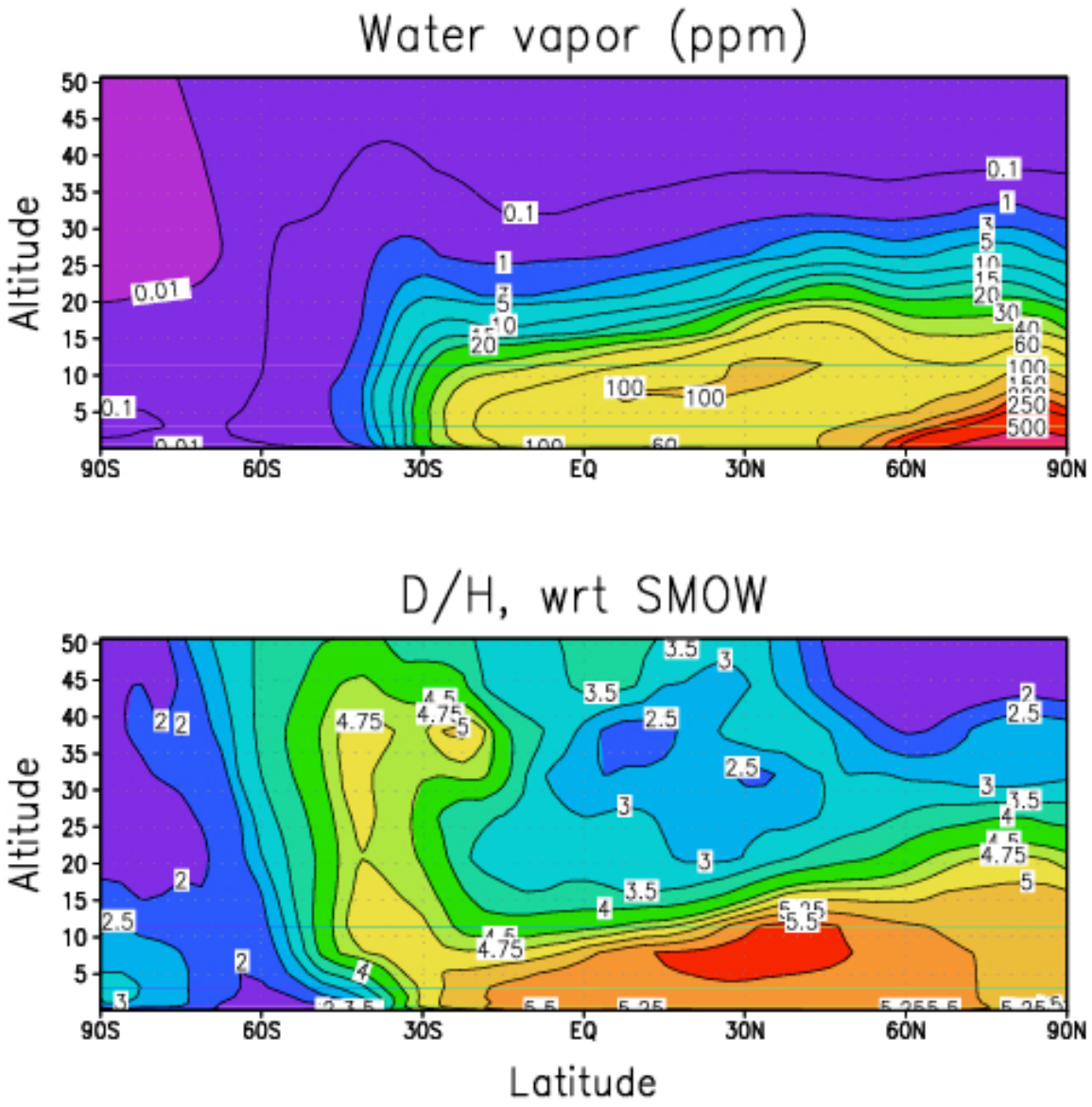

Montmessin et al. (2005)

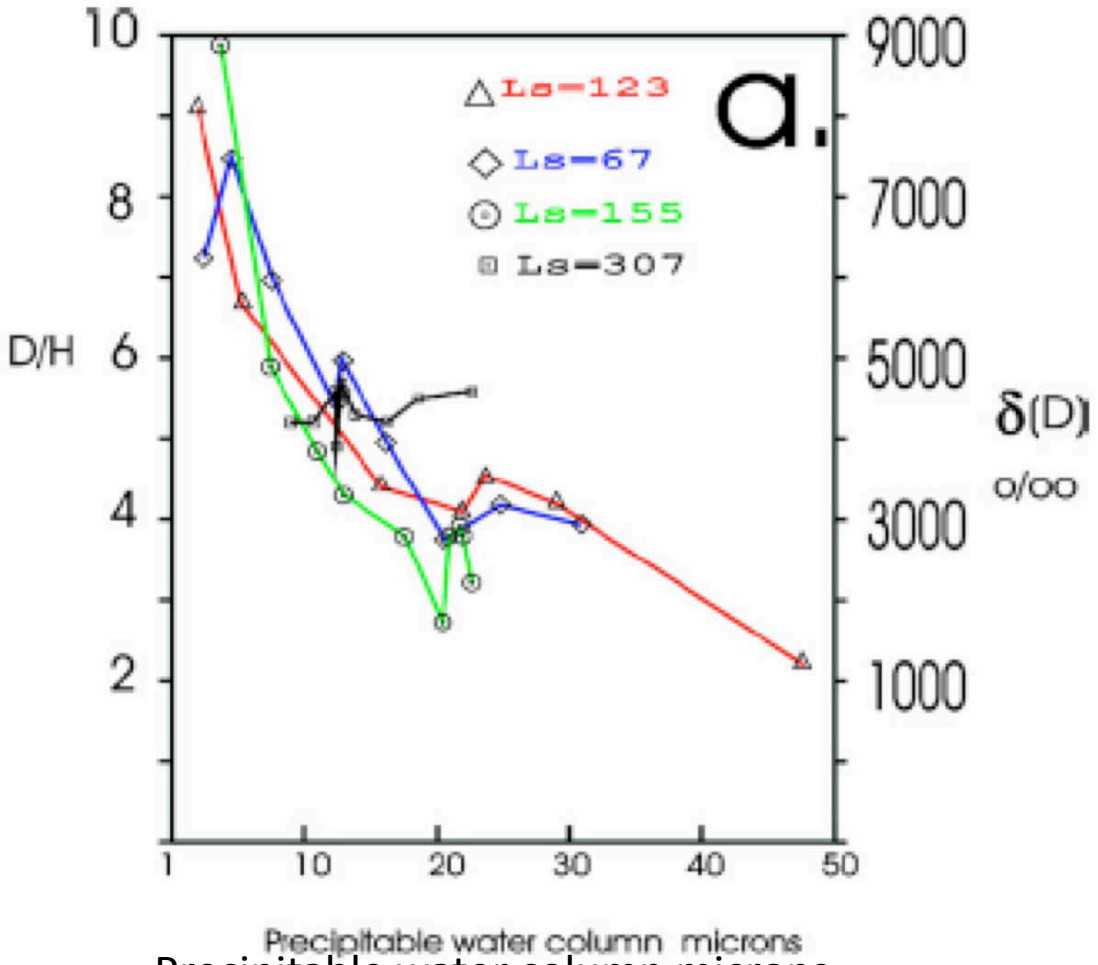

Precipitable water column microns

The smaller the H2O amount, the richer the HDO/H2O.

→Opposite to expectation! (preferential condensation of HDO)

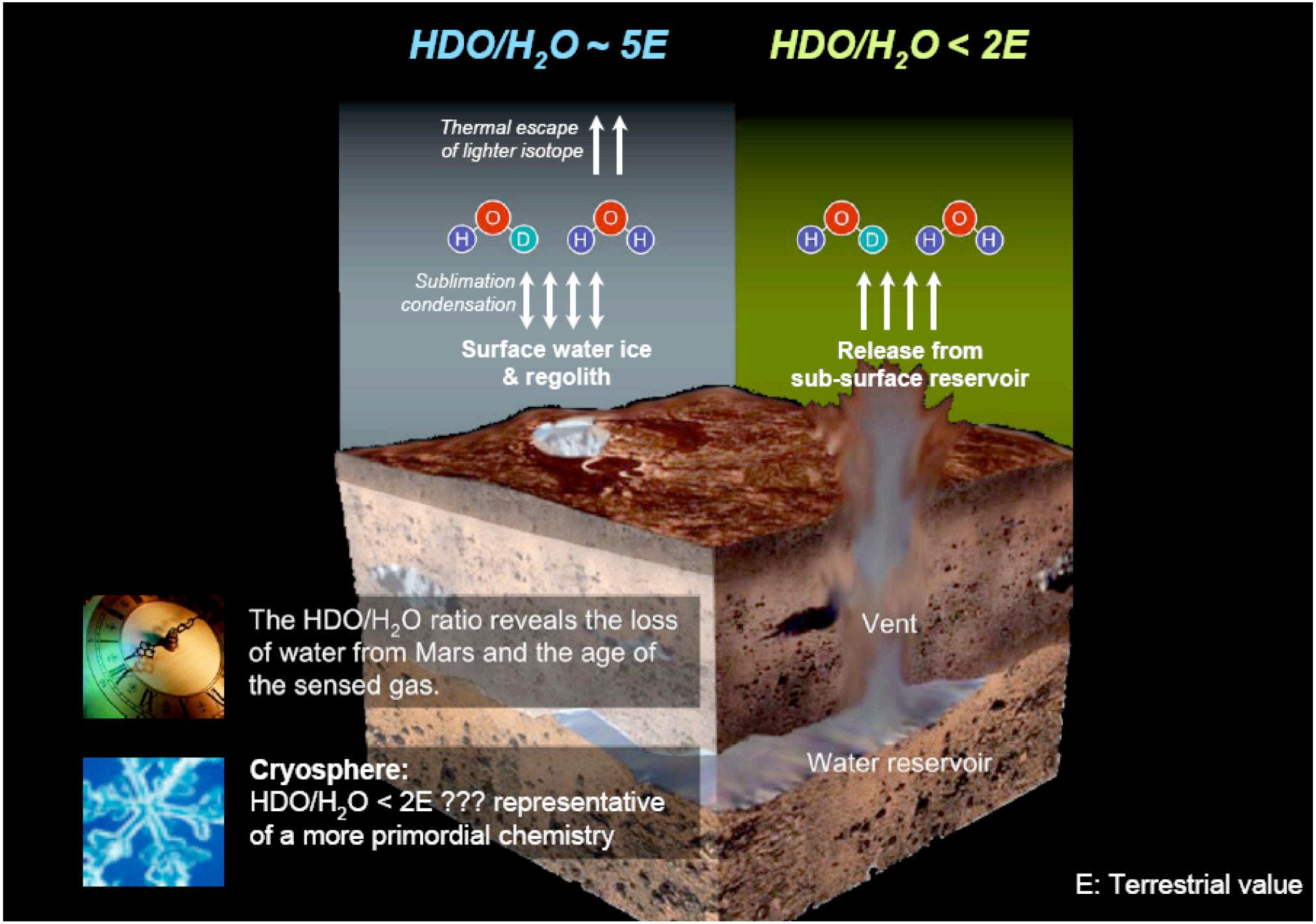
HDO/H2O ~ 5E
HDO/H2O < 2E
Thermal escape of lighter isotope
Sublimation condensation
Surface water ice & regolith
Release from sub-surface reservoir
Vent
Water reservoir
The HDO/H2O ratio reveals the loss of water from Mars and the age of the sensed gas.
Cryosphere:
HDO/H2O < 2E ??? representative of a more primordial chemistry
E: Terrestrial value

大気現象と地下の水との関連

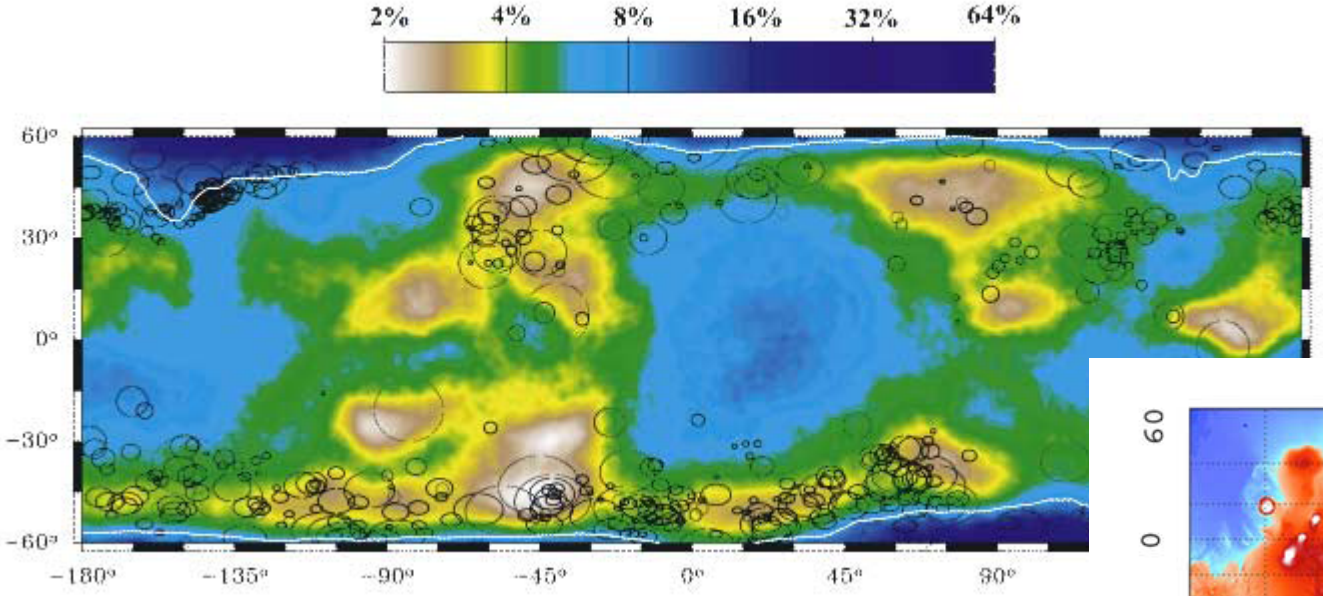

色：Watar Equivalent Hydrogen (WEH)
円：ダストストーム発生地域

Feldman et al. (2005)

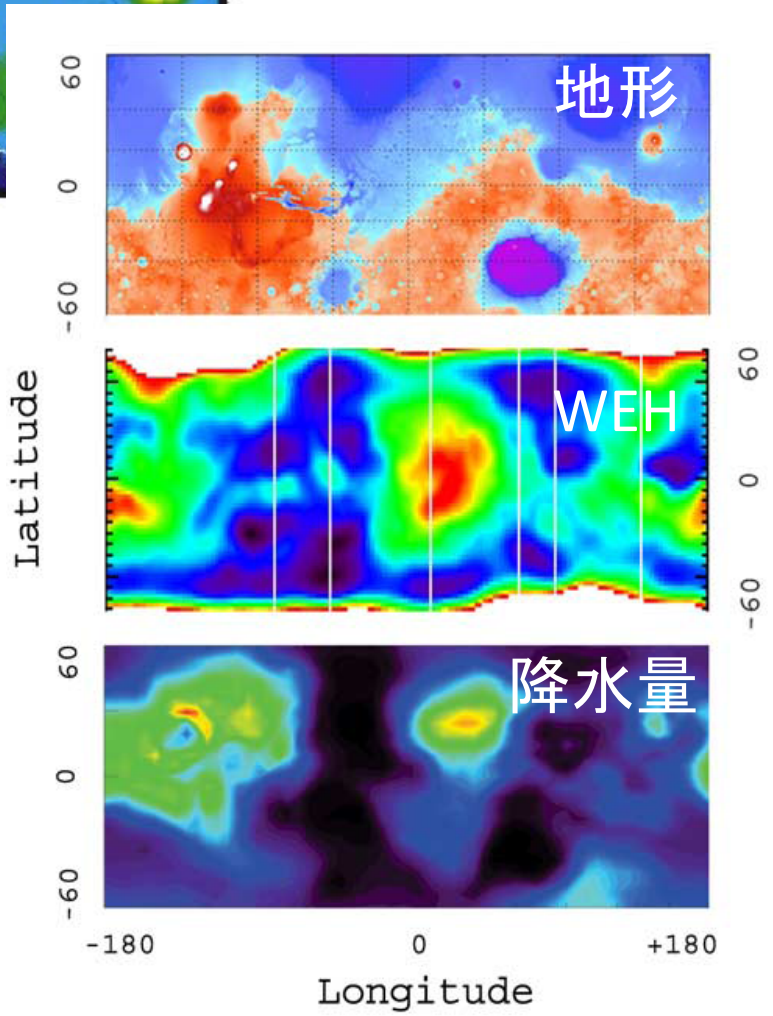

Global dust storm

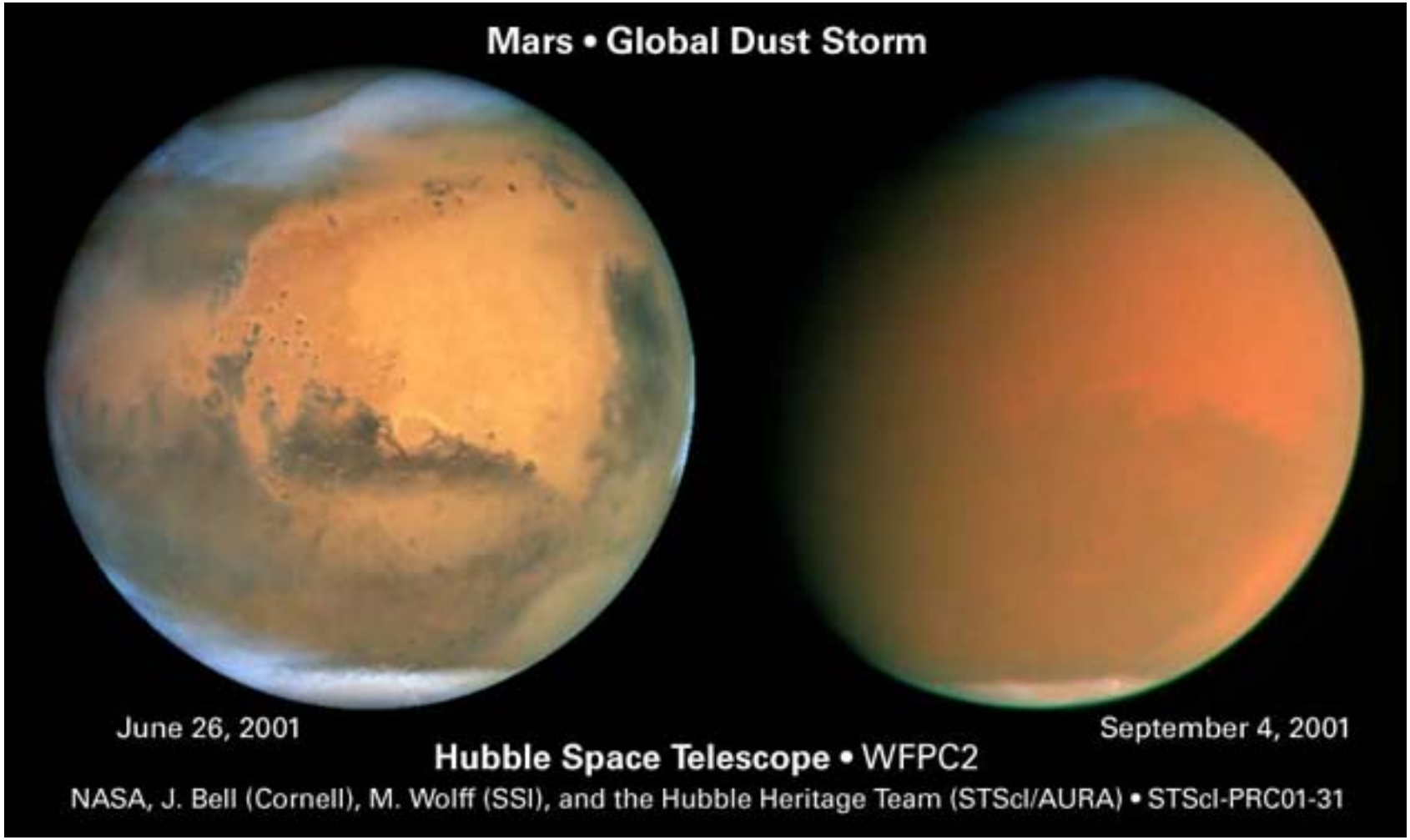

惑星大気のカオス的性質？

– グローバルダストストームが不定期発生

– 平均気温、浮遊ダスト量が年々変動

火星でのダストストーム発生の記録（1905～1990年）

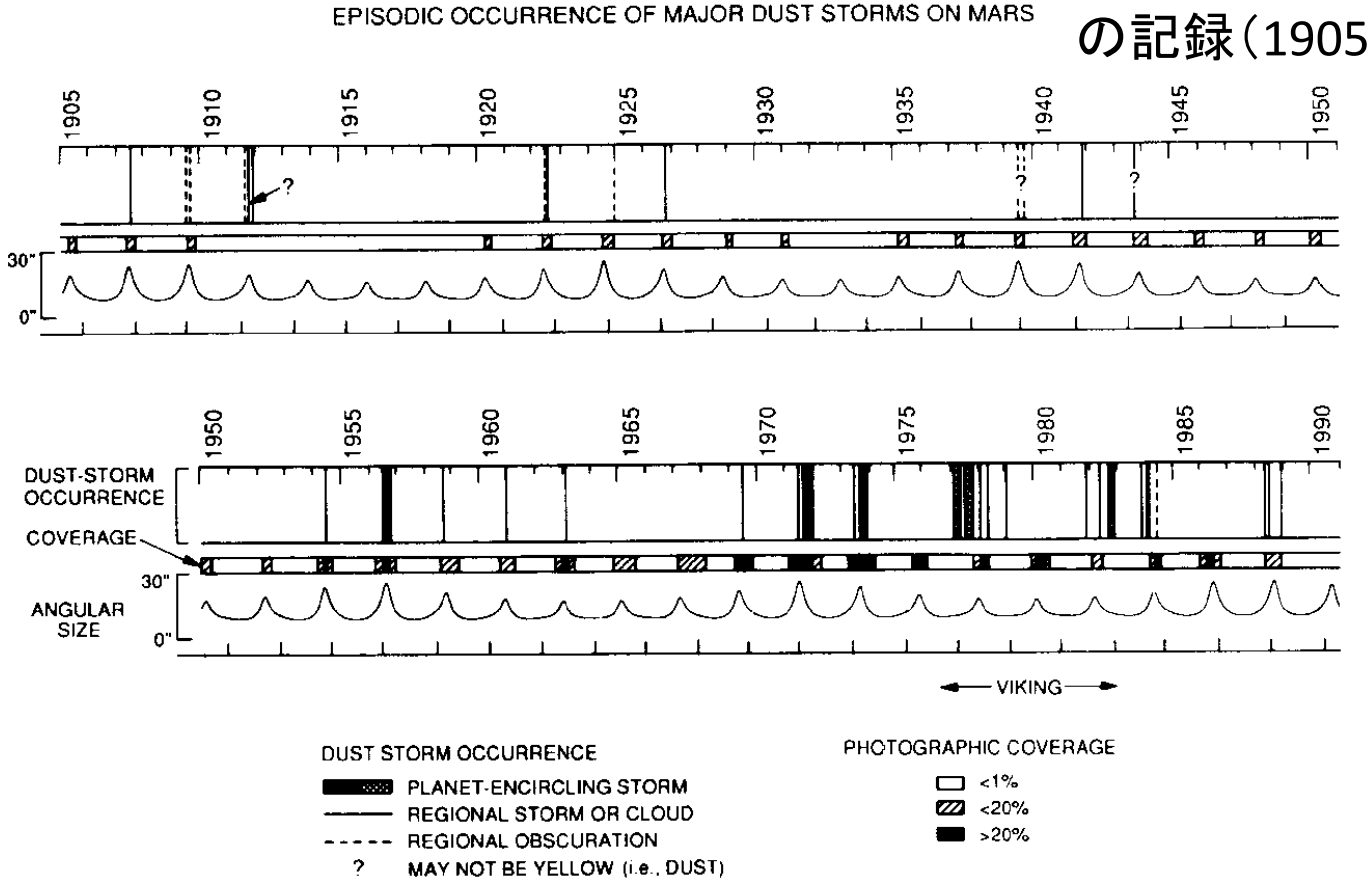

Fig. 7. Timeline of the detection of regional and planet-encircling obscurations, clouds and storms. These events are listed in Table III. Earth dates are indicated at the top, and perihelion

アルベドの変化と気候への影響
Fenton et al. (2007)

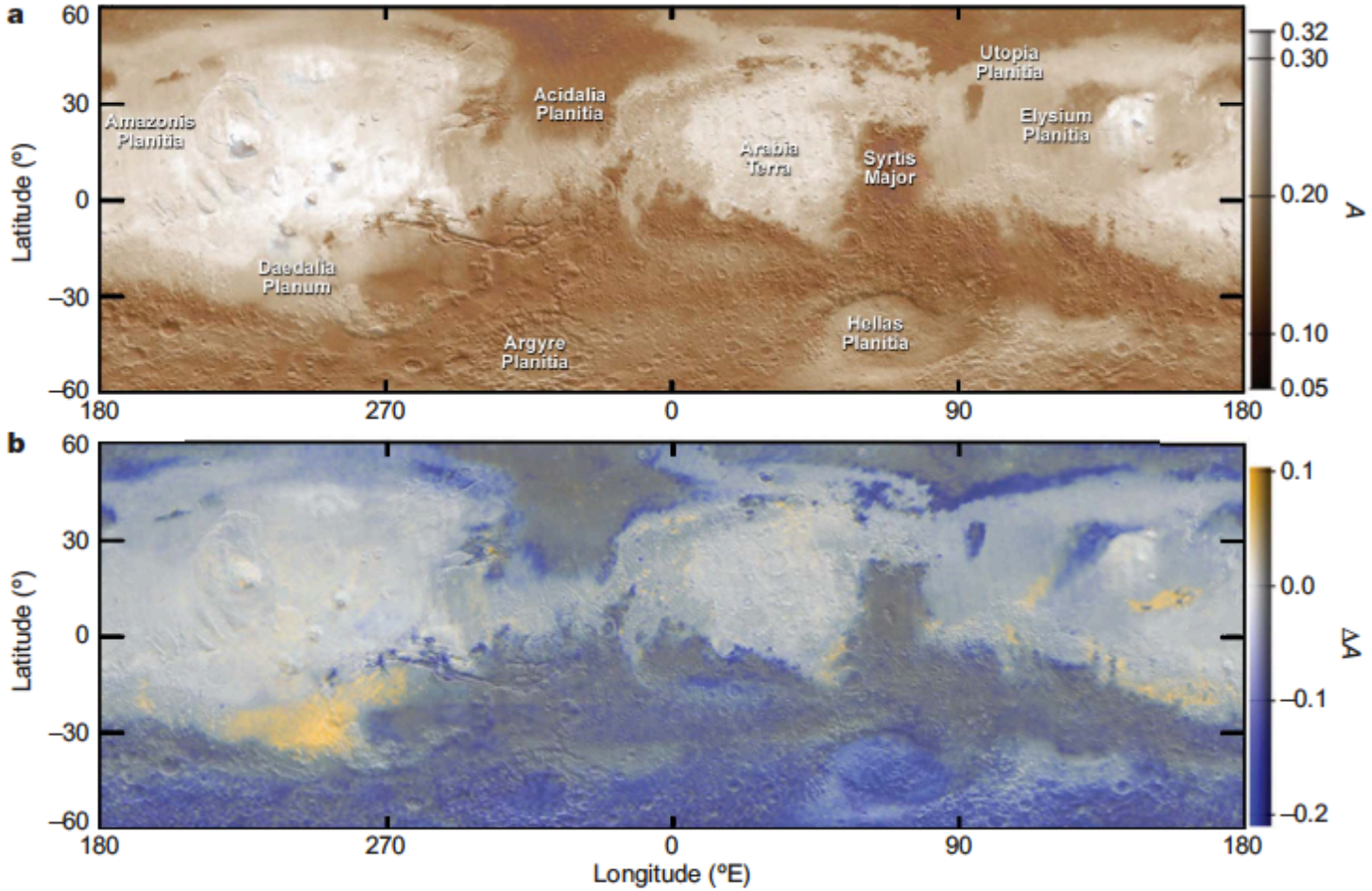

Figure 1 | Albedo and changes in albedo. **a**, Albedo map of Mars superimposed on Mars Orbiter Laser Altimeter (MOLA) shaded relief. Albedos (A) are calculated from the broadband TES bolometer: the rust tint is artificially applied to approximate the appearance of the martian surface. **b**, TES albedos in greyscale superimposed on MOLA shaded relief, with changes (ΔA) relative to the Viking IRTM shown in yellow for relative brightening and blue for relative darkening (see scale on right).

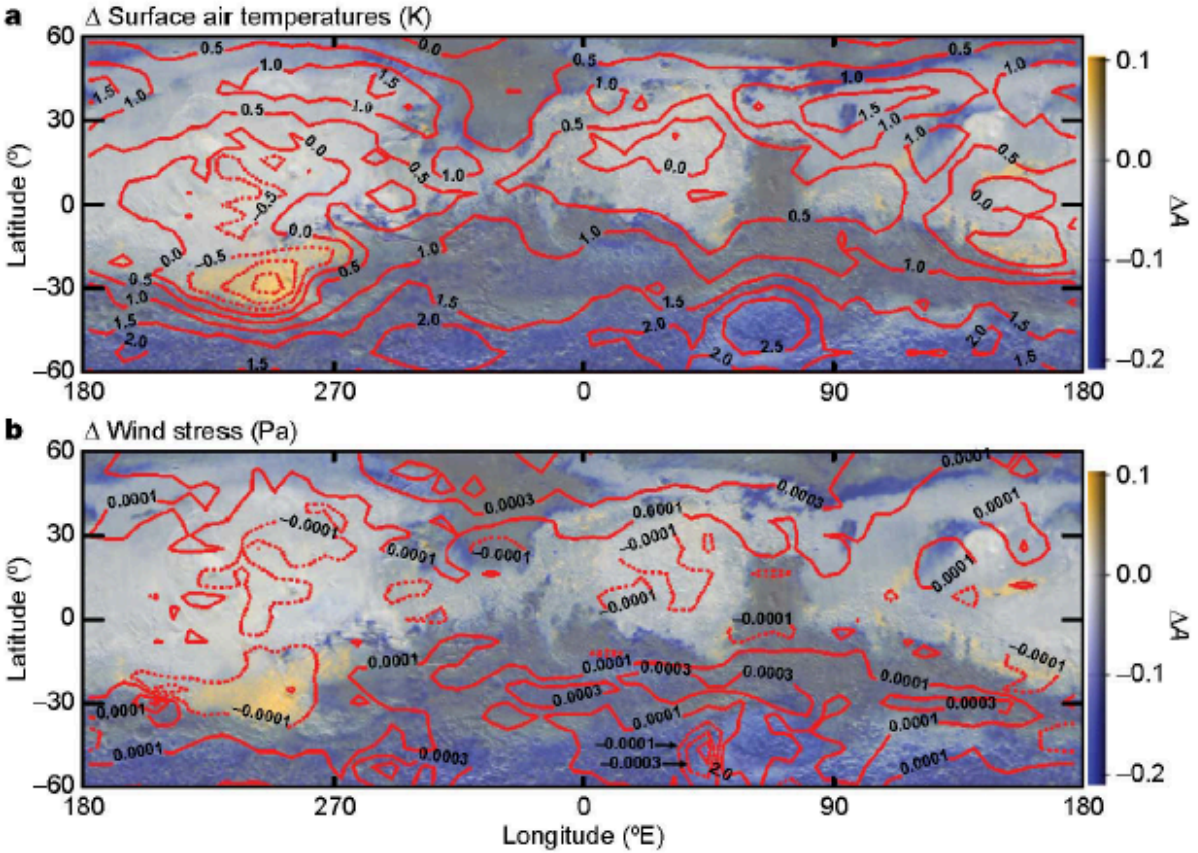

Figure 2 | The effect of albedo changes on air temperature and wind stress. **a**, MGCM-predicted annual-mean change in surface air temperatures (TES−IRTM; contours) on the same plot from Fig. 1. Note the temperature increases over darkened surfaces and temperature decreases over brightened surfaces. **b**, MGCM-predicted annual-mean change in wind stress (TES−IRTM; contours). Note the general correlation of wind stress increases over darkened surfaces and wind stress decreases over brightened surfaces.

放射緩和時間

放射緩和時間＝大気が太陽放射によってあたたまったり惑星放射を放出して冷えたりするのにかかる時間

放射緩和時間は惑星ごとに違う

地球　１００日

火星　３日　　→熱しやすく冷めやすい

金星　５０年　　→熱しにくく冷めにくい

大気の南北循環にかかる時間は１００日くらい

火星では循環があっても大きな温度差が残る。

金星では循環によって温度がよくならされる。

地表ダスト分布の長期変動

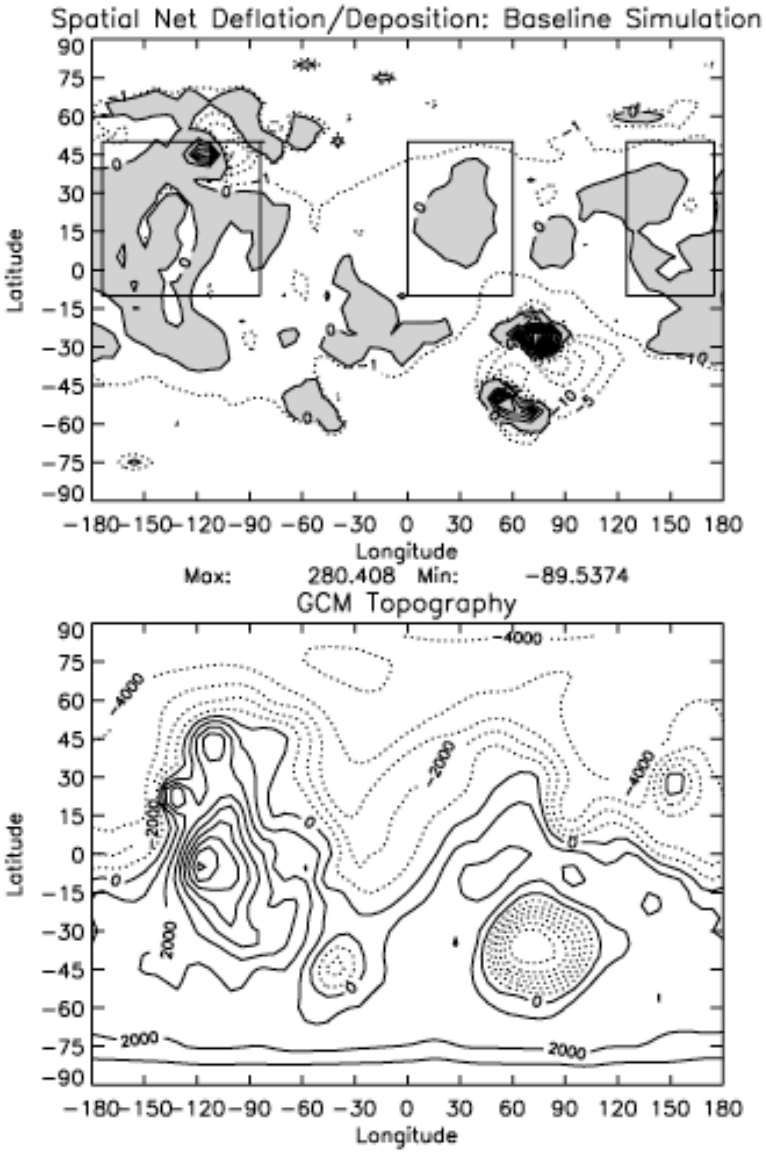

Figure 7. (top) Map of net annual dust deflation (shaded regions) and deposition (nonshaded regions) for the baseline

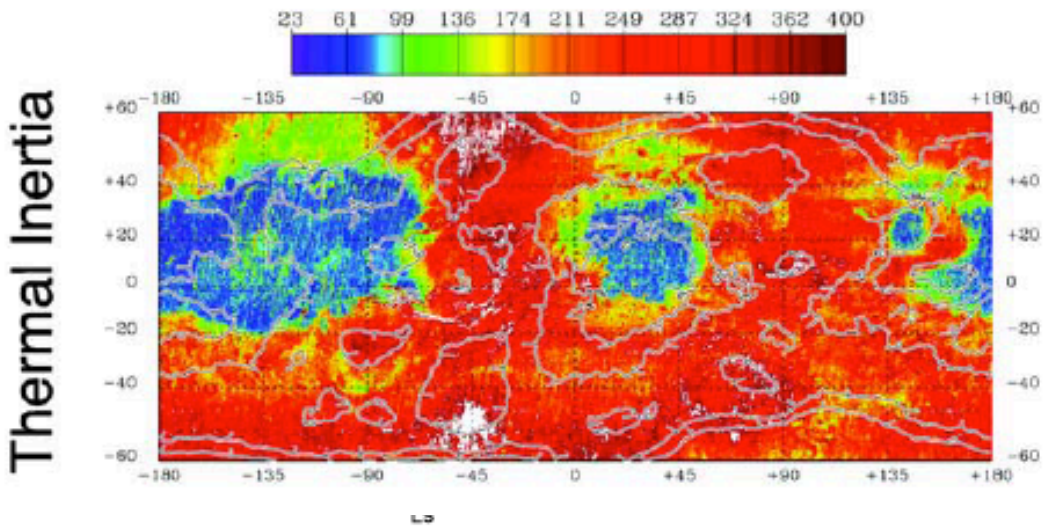

Figure 8. Net surface dust depth deflated (negative) or deposited (positive) as a function of L_s in the north and south regions for the baseline simulation.

each of the dust devil lifting schemes is tuned to match observed northern summer globally and zonally averaged opacities, the simulated opacities during southern spring and summer are low compared to observations (Figure 10).

[49] The threshold-independent dust devil lifting parameterization allows dust to be lifted from a location whenever the surface heat flux is positive (upward heat transfer from the surface to the atmosphere) and the depth of the PBL is nonzero. Therefore dust devil lifting occurs throughout the day. The simulated diurnal peak in the dust devil lifting rate at the grid point nearest the Pathfinder site during the season of the Mars Pathfinder (MPF) mission occurs between 12 pm and 1 pm local time, which is consistent with the observed peak of dust devil occurrence (Figure 11).

有限ダストによる火星GCM

Kahre et al. (2005)

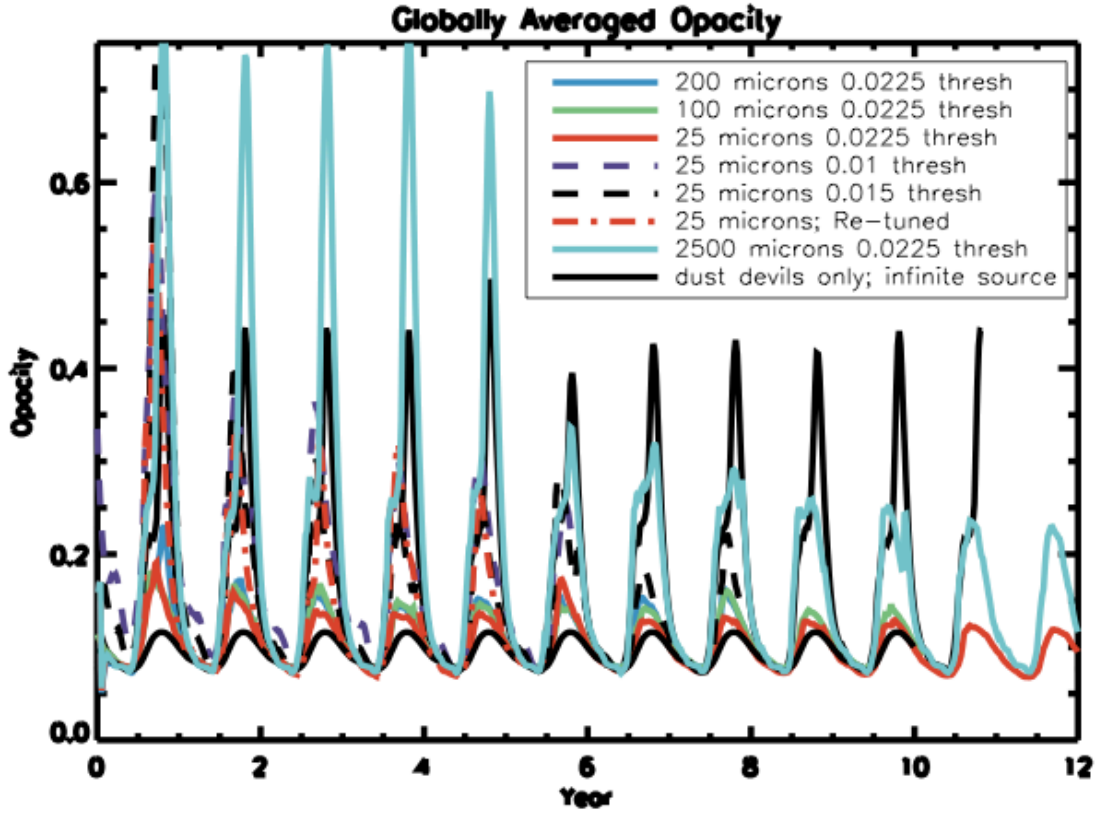

Figure 3. Multi-year globally averaged 9 μm opacity for the infinite surface dust simulation (black solid) the finite surface dust simulations (colored solid and dashed lines).